Research Square

Preprints are preliminary reports that have not undergone peer review.
They should not be considered conclusive, used to inform clinical practice,
or referenced by the media as validated information.

Glycyrrhetinic acid and ethyl acetate extract from Glycyrrhiza glabra mitigates dermal and nasal inflammation: mechanistic insights and nano-formulation strategy

Mona A. Mohammed
on.ibrahim@nrc.sci.eg
National Research Centre
Asmaa Badawy Darwish
National Research Centre
Noha Nazeeh Yassen
National Research Centre
Alyaa Farouk Hessin
National Research Centre
Shaimaa Ali Gad
National Research Centre
Sally Abou Taleb
National Research Centre
Bassant M. M. Ibrahim
National Research Centre

Research Article

Keywords: Glycyrrhiza glabra, phenolic compounds, LC-MS/MS, antioxidant activity, β-cyclodextrin nano-sponges, anti-inflammatory therapy

Posted Date: April 22nd, 2026

DOI: https://doi.org/10.21203/rs.3.rs-9307336/v1

License: This work is licensed under a Creative Commons Attribution 4.0 International License.
Read Full License

Additional Declarations: No competing interests reported.

Orignal Article

Title: Glycyrrhetinic acid and ethyl acetate extract from *Glycyrrhiza glabra* mitigates dermal and nasal inflammation: mechanistic insights and nano-formulation strategy.

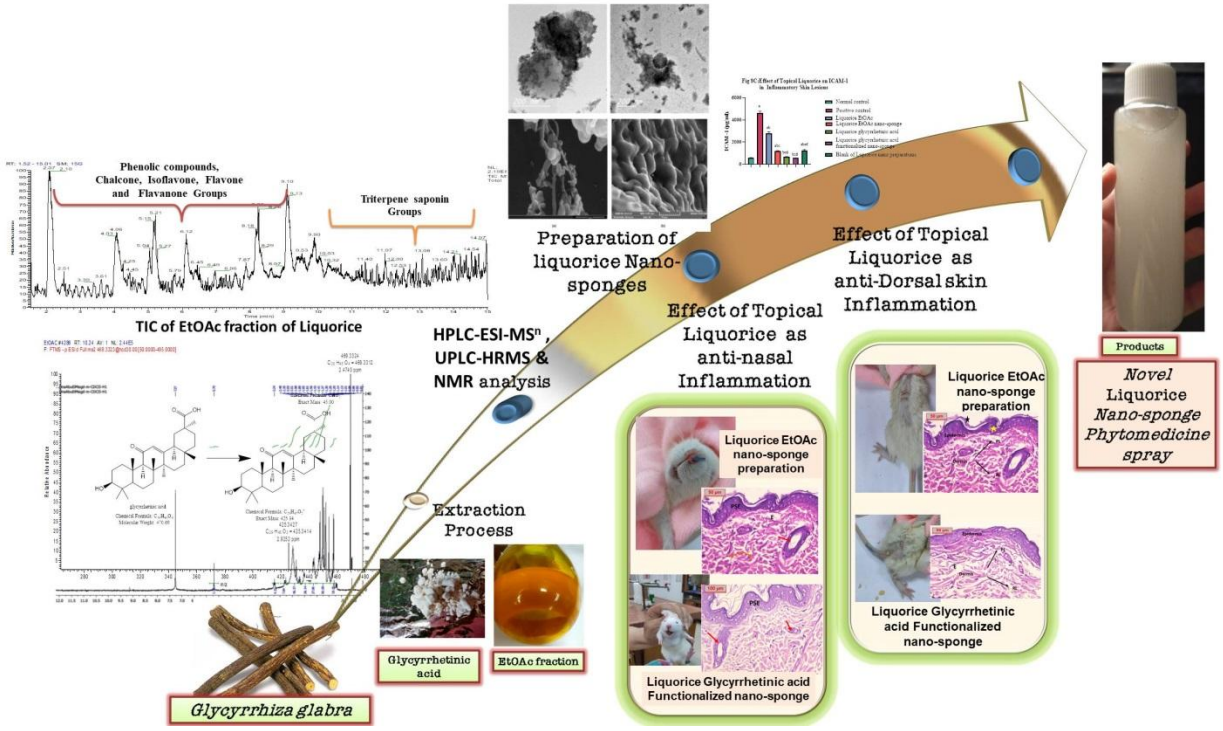
Mona A. Mohammed [1#*], Asmaa Badawy Darwish[2], Noha Nazeeh Yassen[3], Alyaa Farouk Hessin[4], Shaimaa Ali Gad[4], Sally Abou Taleb[2], and Bassant M. M. Ibrahim[4#*]

[1]Medicinal and Aromatic Plants Research Department, Pharmaceutical and Drug Industries Research Institute, National Research Centre, Giza, Egypt
[2]Pharmaceutical Technology Department, Pharmaceutical and Drug Industries Research Institute, National Research Centre, Giza, Egypt.
[3]Pathology Department, Medical Research and Clinical Studies Institute, National Research Centre, Giza, Egypt
[4]Pharmacology Department, Medical Research and Clinical Studies Institute, National Research Centre, Giza, Egypt

***Corresponding author**
[#]Shared equally

Mona A. Mohammed email: monaarafamohammed@yahoo.com, on.ibrahim@nrc.sci.eg
Bassant M. M. Ibrahim email:bmmih1974@gmail.com. bm.ibrahim@nrc.sci.eg.

Graphical Abstract



Abstract

Glycyrrhiza glabra (liquorice) is a widely used medicinal plant for treating inflammatory and respiratory disorders. Its major bioactive compound, glycyrrhetinic acid (GA), exerts anti-inflammatory and immunomodulatory effects through inhibition of 11β-hydroxysteroid dehydrogenase type 2, thereby enhancing local cortisol activity. However, its poor solubility and stability limit its clinical application. In this study, comprehensive metabolite profiling of *G. glabra* roots using UPLC-HRMS led to the identification of sixty-two metabolites, including triterpene saponins, flavonoids, and phenolic acids. GA was successfully isolated and structurally characterized using NMR and LC-MS/MS techniques. To improve its physicochemical properties, GA was incorporated into β-cyclodextrin-based nano-sponges (NSs), which exhibited nano-sized particles (200–289 nm), low polydispersity, high entrapment efficiency, and stable surface charge. In vitro release studies demonstrated a biphasic sustained-release pattern following Higuchi kinetics under both acidic and physiological conditions. Antioxidant assays revealed that the plant extracts displayed stronger activity than pure GA. In vivo evaluation in rat models of dermal and nasal inflammation showed that GA-loaded NSs significantly reduced inflammatory biomarkers, including ICAM-1, IL-β4, and LTB-4, and markedly improved histopathological features, restoring near-normal tissue architecture without signs of irritation. These findings demonstrate that incorporation of GA into β-cyclodextrin nano-sponges enhances its stability, solubility, and therapeutic efficacy, highlighting its potential as a safe and effective natural treatment strategy for skin and nasal inflammatory disorders.

Keywords: *Glycyrrhiza glabra*; phenolic compounds; LC-MS/MS; antioxidant activity; β-cyclodextrin nano-sponges; anti-inflammatory therapy**.**

Abbreviations

2HP-β-CD	Hydroxy propyl-β-Cyclodextrin
AA	Acidic acid
abf	common output format
ABTS	2,2-azinobis(3-ethylbenzothiazoline-6-sulfonic acid)
CA	Citric Acid
CD	Cyclodextrin
CH_2CL_2	Dichloromethane
DCM	Dichloromethane
DLS	dynamic light scattering
DPC	Di-phenyl Carbonate
DPPH	2,2-diphenyl-1-picrylhydrazyl
EE%	Entrapment Efficiency
Epi-βCD	Polymerized-β-Cyclodextrin
EtOAc	Ethyl acetate
FC reagent	Folin Ciocalteu reagent
FTIR	Fourier Transform Infrared Spectroscopy
GA	Gallic acid
H&E	Hematoxylin and Eosin
HPβCD	Hydroxypropyl β-Cyclodextrin
ICAM-1	Intracellular adhesion molecule-1
ILβ4	Interleukinβ 4
KH_2PO_4	potassium dihydrogen phosphate
L3	Liquorice EtOAc nano-sponge
L4	glycyrrhetinic acid nano-sponge
LC%	Loading Capacity
LCMSMS	Liquid chromatography–mass spectrometry
LTB_4	Leukotriene B4
Na_2HPO_4	Anhydrous disodium hydrogen phosphates
n-BuOH	n-Butanol
NSs	Nanosponges
PDI	polydispersity index
Pet. ether	Petroleum ether
PL	papillary layer
PS	particle size
PSE	pseudostratified epithelium
Q_{6h}	Percent total Liquorice released after 6 h.
RI	Retention Indices
RL	reticular layer
RPM	Rotations per minute
SEM	Scanning Electron Microscopy
TEM	Transmission Electron Microscopy
UPLC-HESI-MS/MS	Ultra-Performance Liquid Chromatography- Heated Electrospray Ionization- mass spectrometry
UPLC-HRMS	Ultra-Performance Liquid Chromatography- High Resolution Mass Spectrometry
VS	Vesicle Size
ZP	Zeta Potential

1. Introduction

Liquorice a perennial species belonging to the family Leguminosae, ranks among the most extensively utilized medicinal herbs worldwide. For centuries, it has been employed for its wide spectrum of pharmacological effects, including antiulcer, anti-inflammatory [1], antiallergic, antispasmodic, expectorant, antidepressant [2], antifungal, antiviral [3], and antioxidant properties. Liquorice is frequently used in the food industry as a natural flavoring and sweetener, in addition to its therapeutic uses. Its safety profile is The U. S. Food and Drug Administration has given it the "generally recognized as safe" (GRAS) certification, and it is well established. The pharmacological activities of Liquorice are mainly attributed to triterpene saponins, particularly glycyrrhizic acid, and phenolic compounds such as flavanones, flavones, isoflavones and chalcones [4]. The chemical profile of Liquorice can be characterized using advanced analytical techniques such as LC-MSMS. A rapid LC-MSMS analytical technique has been developed to simultaneously quantify key compounds including glycyrrhizic acid, glycyrrhetinic acid, and others in complex mixtures[5]. The roots are highly enriched in triterpenoid saponins, notably glycyrrhizic acid often referred to as glycyrrhizin and its pharmacologically versatile aglycone, glycyrrhetinic acid [6]. Glycyrrhizic acid undergoes hydrolysis in the gastrointestinal tract by microbiota, yielding glycyrrhetinic acid, the main systemic metabolite and mediator of Liquorice-derived bioactivity [7]. Together, glycyrrhizic acid, glycyrrhizin, and glycyrrhetinic acid emerge as dominant, interrelated bioactive markers vital for the authentication and quality control of *Glycyrrhiza glabra* preparations. Glycyrrhetinic acid primarily exerts its pharmacological actions by inhibiting the enzyme 11β-hydroxysteroid dehydrogenase type 2 (11β-HSD2), which catalyzes the conversion of active cortisol into its inactive form, cortisone [8]. Inhibition of 11β-HSD2 elevates local cortisol levels, thereby enhancing glucocorticoid receptor activation and exerting potent anti-inflammatory effects [9]. Moreover, excess cortisol resulting from 11β-HSD2 inhibition can bind to mineralocorticoid receptors (MR), mimicking aldosterone activity and promoting sodium retention, potassium excretion, and increased blood pressure [10]. This mechanism explains the hypertensive and electrolyte imbalance effects observed in individuals consuming high doses of Liquorice or its derivatives [11]. Drug delivery systems represent a significant advancement in overcoming problems associated with poor solubility and uncontrolled release of therapeutic agents [12]. Nanotechnology, considered one of the most revolutionary scientific advancements since the industrial era [13], enables the manipulation of materials at the nanoscale to design carriers with superior properties. Naturally occurring polysaccharides such as cyclodextrins are particularly attractive due to their biocompatibility, biodegradability, and cost-effectiveness [14]. Cyclodextrins can enclose guest molecules within their internal cavity, thereby improving solubility, stability, and bioavailability [15, 16]. When crosslinked with suitable agents, cyclodextrins form nanosponges nanostructured [17], three-dimensional, mesh-like systems with both hydrophilic external branches and hydrophobic inner cavities[18]. These structures can encapsulate a wide range of molecules, enhance solubility of hydrophilic and lipophilic drugs[19], prolong drug release, and ultimately improve bioavailability [20]. Inflammation is a natural defense response to trauma, whether chemical or mechanical, and is characterized by edema, redness, and pain. However, edema can be particularly dangerous when it occurs in the respiratory airways [21]. Conventional anti-inflammatory agents such as glucocorticoids remain the mainstay of treatment but are associated with significant side effects, leading to poor patient compliance [22]. This has fueled growing interest in herbal therapies, which are generally safer and better tolerated [21]. Liquorice, due to its active constituents such as glycyrrhizic acid, is considered one of the most potent anti-

inflammatory herbs and has shown promising efficacy in both respiratory and skin inflammation owing to its immunomodulatory effects [23]. This study aims to evaluate new formulations of Liquorice extracts for the treatment of chemically and mechanically induced skin inflammation. To maximize therapeutic efficacy, Liquorice will be administered via dual routes intra-nasally and topically on wounds through a locally acting nanocomposite delivery system designed to enhance its anti-inflammatory potential and alleviate associated signs and symptoms.

2. Material and Methods

2.1. Materials and Analytical Reagents

Liquorice samples were sourced from Harraz, a local herbal supplier in Egypt, and were authenticated and deposited at the NRC Herbarium under voucher number M297 [24]. The powder was made from the leaves by drying them in the shade and then grinding them into a fine powder. We bought FC reagent and Trolox from Sigma-Aldrich (Germany), and GA from Acros Organics (Belgium). We got ABTS and DPPH reagents from Sigma-Aldrich for our antioxidant assays. Fisher Scientific (UK) provided Fisher Scientific (UK) with analytical grade solvents and chemicals. Hydroxypropyl β-cyclodextrin (HPβCD; KLEPTOSE HPB, MW 1380 Da) and polymerized β-cyclodextrin (Epi-βCD) were generously supplied by Roquette (France). Diphenyl carbonate (DPC) was procured from Acros Organics (Belgium), and prednisolone was obtained from Sigma (USA). Potassium dihydrogen phosphate (KH_2PO_4), disodium hydrogen phosphate (Na_2HPO_4), and cellulose dialysis membranes were sourced from El-Gomhouria (Egypt) and Sigma-Aldrich (Steinheim, Germany). All additional reagents and solvents were analytical grade and used as supplied.

2.2. Extraction of liquorice and Isolation of Glycyrrhetinic acid

Extraction is an important step in separating bioactive components from plants. The most prevalent technique is solvent extraction, which uses solvents such as pet.ether, CH_2CL_2, EtOAc, BuOH, and water. The procedure includes solvent penetration, solute dissolving, diffusion from the plant matrix, and collection. Solvent characteristics, particle size, solvent to solid ratio, temperature, and time all affect extraction efficiency.

A total alcohol extracts (by soaking 48h at room temperature then evaporate till dryness) is treated with H_2SO_4 to precipitate light brown sediment, which is washed with water and is extracted by alcohol to isolate glycyrrhizin potassium salt. The Glycyrrhizin is precipitated by adding KOH solution to the extract which is filtered and crystallized twice in acetic acid. The salt is hydrolyzed with H_2SO_4 to give crude glycyrrhetinic acid that is acetylated by acetic anhydride. The resulting cake is then purified by CH_2CL_2 then is hydrolyzed by NaOH solution to obtain white glycyrrhetinic acid.

2.3. Phytochemical detection methods

The detection of volatile constituents was performed on 10 g of the sample following the method described by [25]. Carbohydrates and glycosides were identified in the methanolic extract using α-naphthol and sulfuric acid reagent, as outlined by [26]. Tannins were quantified using Shellard's procedure [27]. For alkaloid detection, one milliliter of the methanolic extract filtrate was reacted with 2.5 mL of Dragendorff's reagent [28]. Flavonoids were first detected by the production of a yellow tint but the presence of a red color after supplementation of Magnesium and hydrochloric acid suggested the presence of flavanones and/or flavonols [29]. Saponins were suspected to be present due to the production of a stable froth that lasted for

around 30 minutes [27]. Unsaturated sterols and/or triterpenes were detected according to the method of [30].

2.4.Secondary Metabolite Profiling of Liquorice roots using LC-MS, UPLC-HRMS techniques and Data processing

The major metabolites in Liquorice root samples were profiled following extraction using various organic solvents. This strategy aimed to differentiate secondary metabolites based on the "like dissolves like" principle while considering possible degradation during extraction. Metabolite profiling was performed using an ion-trap MS (Esquire 3000, Bruker Daltonics) with ESI in ± modes (m/z 150–3000, scan rate 13,000 m/z/s) [31, 32]. High-resolution UPLC–Q-Exactive Orbitrap (Thermo Fisher) analysis employed a BEH Shield RP18 column (150 × 2.1 mm, 1.7 μm) and a gradient of 0.1% formic acid: water (A) and acetonitrile (B): 5 - 50% B (0 - 14 min), 50 - 98% B (14 - 20 min), hold 5 min, re-equilibrate 3 min, at 0.4 mL/min. Source parameters: HESI ±3.0 kV, sheath gas 48 L/min, aux gas 13 L/min, capillary 250 °C, heater 380 °C. CID was applied at 15 eV. Data were processed in MS-DIAL 4.60 (ABF format) and compounds annotated via MassBank, Knapsack, Fiehn BinBase, LipidBlast, and RIKEN databases [33, 34].

2.5. Determination of the Calibration curve of Liquorice extracts

A calibration curve for the Liquorice extracts and glycyrrhetinic acid was prepared in PBS at pH 5.5 and pH 7.4, using a stock solution of 100 μg/ml. Serial dilutions were used as 2; 4; 6; 8; and 10 ml aliquots of the stock solution, and each was adjusted to an end volume of 10 ml with PBS of the respective pH.

2.6.Preparation of Nano-sponges

NSs were synthesized using a modified ultrasound-assisted method. HPβCD (polymer) and DPC (cross-linker) were mixed in distilled water at different molar ratios (1:1; 1:4; and 4:1) (Table 1). The mixture was sonicated at 90 °C [35, 36], homogenized (12,000 rpm, 7 min), and centrifuged (6,000 rpm, 30 min). Liquorice extract was added, shaken overnight (150 rpm), re-sonicated, and centrifuged again. The final product was freeze dried and stored at 25 °C [37].

Table 1: Physicochemical properties, composition, and entrapment efficiency of Liquorice-based nano-sponge formulations

Code	Molar Ratio			EE% ± SD	LC% ±SD	VS ± SD (nm)	ZP ± SD (mV)	PDI
	2HPβCD	Epi-βCD	DPC					
L1	1	-	1	98.93± 7.22	8.62 ± 1.08	200.6 ± 3.91	-16.8 ± 4.47	0.551
L2	1	-	4	99.79 ± 4.09	10.89 ± 1.85	232.1 ± 6.25	-20.1 ± 5.11	0.562
L3	4	-	1	100.07 ± 3.68	31.37 ± 1.79	289.4 ± 4.83	-31.2 ± 5.02	0.505
L4	-	4	1	100.02 ± 5.17	12.86± 2.96	149.4± 3.72	-24.8 ± 4.99	0.618

 # Hydroxy propyl-β-cyclodextrin (2HP-βCD), Polymerized-β-cyclodextrin (Epi-βCD) and Diphenyl carbonate(DPC)

2.7. Determination of EE% and LC% of NSs.

Nanosponges with 10 mg of Liquorice extract and glycyrrhetinic acid were diluted in 100 ml of phosphate buffer (pH 7. 4) and agitated for 50 minutes. After filtering (0.22 μm), the A UV–Vis

spectrophotometer (Shimadzu Pharma Spec 1700) was used to examine the samples at λ_{max} = 321.2 nm. The EE% and LC% were calculated using the following formulas [38]:

EE% = (Drug in NSs/Initial drug) * 100.

LC% = (Drug in NSs / Total NS weight) * 100.

2.8. Measurement of Vesicle Size, Polydispersity Index (PDI), and Zeta Potential (ZP).

The particle size, PDI, and ZP of the formulations were measured using a Zetasizer Nano ZS (Malvern Instruments, UK). Measurements were taken at ambient temperature using dynamic light scattering (DLS), which is based on laser diffraction. The correlation function of the scattered light intensity was measured at a constant scattering angle of 90° [39].

2.9. Measurement of the Optimized Formulations.

Based on preliminary experiments, the molar ratio that produced the most favorable EE%, PS, and ZP values was selected as the optimized formulation. A novel nanosponge system was then prepared using EPI-βCD and DPC at the identified molar ratio, and loaded with Liquorice EtOAc extract (formulation L4, Table 1). The preparation and characterization followed the same methods described above.

2.10. Surface Morphology *(*SEM and TEM) and FT-IR Spectroscopy

The morphology of optimized NSs was examined by TEM (JEM-2100, JEOL, Japan) after staining with 1% phosphotungstic acid [20]. SEM (Quanta FEG 250, Thermo Fisher, Czech Republic) was used to study surface structure, with gold-coated freeze-dried samples imaged at 20 kV and 10 mm working distance [39].

FT-IR analysis was performed using a JASCO 6100 spectrophotometer (Tokyo, Japan) to assess potential chemical interactions between components in the optimized formulations. Samples of HPβCD, EPI-βCD, DPC, Liquorice extract, and glycyrrhetinic acid freeze-dried NSs (L3 and L4) were each blended with KBr and compressed into pellets under 200 kg/cm² for two minutes using a hydraulic press. The spectra were recorded in the 4000–400 cm^{-1} range against a KBr blank (Table 2).

Table 2: Release kinetics parameters and corresponding correlation coefficients of Liquorice from the optimized NSs formulations.

Code	Q_{6h} ± SD (%)	0-Order	1-Order	Higuchi	Peppas	
		R^2			R^2	N
L3 in acidic medium	40.32±0.87	0.6585	0.5829	0.7096	0.9309	0.1572
L4 in acidic medium	19.48±1.65	0.5733	0.4694	0.8758	0.9487	0.1878
L3 in alkaline medium	60.14±2.17	0.8561	0.8232	0.7866	0.9528	0.2541
L4 in alkaline medium	55.25±2.23	0.5066	0.4271	0.7391	0.9103	0.1548

Q_{6h}: Percent total Liquorice released after 6 h.

2.11. *In-vitro* release Study

Liquorice EtOAc extract and glycyrrhetinic acid release from NSs (L3, L4) was evaluated in PBS (pH 5.5, 7.4) using dialysis bags (MWCO 12–14 kDa, Sigma-Aldrich). Bags containing 2 mg formulation were incubated in 100 mL PBS at 37.0 ± 0.50°C, 100 rpm. Samples

were withdrawn at intervals, replaced with fresh medium, and analyzed spectrophotometrically. Cumulative release was calculated, and kinetics was fitted to 0-order, 1-order, Higuchi, and Korsmeyer–Peppas models [40].

2.12. Antioxidants Activity of Extracts Different Plants (*In vitro* study).

The antioxidant activity of different extracts from Liquorice and two other plants was assessed *in vitro* using $ABTS^{\cdot+}$ and $DPPH^{\cdot-}$ radical assays. Total methanol extracts and fractions (Pet. ether, DCM, EtOAc, n-BuOH, H_2O) were tested at concentrations ranging from 0.5-30 µg/mL. AA and Trolox served as standards group. DPPH was measured by mixing 2 mL extract (100 µg/mL) with 2 mL DPPH (100 µM in methanol), incubating in the dark room for 15 min, and recording absorbance at 517nm. Inhibition (%) was calculated as: [(A_control – A_sample) / A_control] × 100 [41]. $ABTS^{\bullet+}$ was generated by reacting 7 mM ABTS with 2.45 mM $K_2S_2O_8$ for 12–16 h and diluting to an absorbance of 0.70 ± 0.05 at 734nm. Then, 50 µL sample or Trolox was mixed with 1 mL $ABTS^{\bullet+}$ solution, and absorbance was measured at 734 nm (1 - 6 min). Activity was expressed relative to AA and Trolox standards [42].

2.13. Determination of Skin Sensitivity to Liquorice EtOAc, Liquorice EtOAc Nano-sponge, Liquorice Glycyrrhetinic acid and Liquorice Glycyrrhetinic acid Functionalized Nano-sponge:

Twenty male rats were utilized and equally divided into four groups. Twenty- four hours before the test, dorsal body hair was shaved, with caution not to abrade the skin. The tested substances were administered over a definite skin area (≈ 4 cm^2). They were initially placed on a gauze patch and subsequently applied to the skin under a semi-occlusive dressing for duration of four hours.

Up to three test patches were sequentially applied to each animal. The first patch was removed after 3 minutes; as no serious skin reaction was observed, a second patch was applied at a different site and removed after 1 hour. Based on the absence of adverse effects, exposure was extended to 4 hours with a third patch, after which the response was graded. The test substance's potential to cause skin irritation was then assessed. Following the 4^{th} hour exposure, any residual compound was carefully removed, without disturbing the skin response or epidermal integrity. Animals were subsequently examined for signs of erythema and oedema [43].

2.14. Efficacy Study of the Therapeutic effects of Local application of Liquorice EtOAc, Liquorice EtOAc nano-sponge, Liquorice Glycyrrhetinic acid and Liquorice Glycyrrhetinic acid Functionalized Nano-sponge on Skin Inflammation in rats:

The dorsal aspects of thirty-five male rats were shaved then the animals were distributed into seven groups (each consisted of five rats). The groups were classified as follows:

-Normal group: for which hair shaving only was done.

-Nasal inflammation and corporal skin inflammation of the dorsal body aspect, were induced in the other rats as follows: Thirty rats were scratched gently with a sterilized needle tip to induce superficial wound together with instillation of 0.05 ml of 1750 nmol/1 capsaicin solution into each nostril of every rat. Capsaicin solution was prepared by dissolving capsaicin in a vehicle containing equal volumes of 10% ethanol, 10% Tween 80 and 80% saline [44]. Then the rats were subdivided into six groups as follows:

-Positive control (Untreated) group: Rats that didn't receive treatment.

-Four treated groups: 1st was treated with Liquorice EtOAc extract, 2nd was treated with Liquorice EtOAc nano-sponge, 3rd was treated with Liquorice Glycyrrhetinic acid and 4th was treated with Liquorice Glycyrrhetinic acid functionalized nano-sponge.
Each treatment was applied in the form of paint on the dorsal skin lesions and nasal drops in each nostril. The doses of either the paint or the nasal drop in each nostril were 0.25 ml (each one ml of lotion contained one mg of tested substance).

After twenty-four hours, macroscopic assessment of the noses by inspection was done by giving a grading score, where 0= normal nostril appearance without swelling or redness, 1= nasal redness, 2= nasal oedema with redness (0 is the best and 2 is the worst grade). Assessment of the dorsal skin scratch healing by inspection was given the following score: 0= intact dorsal skin, 1= formation of brownish fibrous tissue and reduction in the size of the scratch denoting the beginning of healing, 2=beginning of formation of faint brownish fibrous tissue at the site of scratches, 3= red scratches with surrounding oedema without development of fibrous tissue (0 is the best and 3 is the worst grade).
After macroscopic evaluation, blood samples were collected from retro orbital plexus of veins of all rats, and were processed for performing the biochemical analysis in sera [45]. ICAM-1, IL-β4 and LT-B4 were measured in serum by using high grade ELISA kits, and the maneuvers followed the manufacturer's guidelines.
Dorsal skin and nasal tissues were collected, fixed in 10% neutral-buffered formalin (≥12 h), rinsed, dehydrated in graded ethanol, cleared with xylene, and embedded in paraffin. Serial 3 µm sections were stained with H&E [46]. Microscopic examination and imaging were performed using an Olympus CX41 microscope with an SC100 digital camera (Pathology Lab, NRC). Photomicrographs were processed with Adobe Photoshop v8.0.

2.15. Statistical Analysis

Data were expressed as means ± standard error (SE). Statistical analyses were performed using "One-way Analysis of Variance (ANOVA)" followed by "Tukey–Kramer's" post hoc test, with significance values $p \leq 0.001$. All computations were conducted using Graph Pad Prism (version 8).

3. Results

3.1. Plant extraction and Phytochemical screening

Plant materials were macerated in 70% methanol for 48 h at room temperature. The collected extracts were evaporated to dryness under vacuum at 40 °C, suspended in distilled water, and left overnight. Successive partitioning was carried out with DCM, EtOAc, and n-BuOH using a rotary evaporator. All fractions were filtered through Whatman No. 54 paper [47].

Phytochemical screening of Liquorice and its fractions revealed diverse secondary metabolites with varying distribution based on solvent polarity. Carbohydrates, tannins, flavonoids, and saponins were abundant in the total extract, butanol, and aqueous fractions, indicating their polar nature. Non-polar fractions (Pet. ether, CH_2Cl_2) were rich in sterols, triterpenes, and alkaloids. Saponins were present across most fractions, showing both polar and semi-polar solubility. Coumarins were detected mainly in CH_2Cl_2 and butanol, while flavonoids were more prominent in butanol and EtOAc. Notably, volatile oils were absent in all tested fractions shown in Table S1.

3.2.Compound Characterization

The isolated compound was identified as glycyrrhetinic acid, a pentacyclic triterpenoid classified under the oleanane type. This identification was established through detailed analysis of its ^{1}H & ^{13}C NMR spectra (Figure S1) and LC-MSMS.

The ^{1}H NMR spectrum exhibited characteristic signals in the olefinic and aromatic regions, specifically between δ 5.70 and 7.84 ppm, which are indicative of unsaturated hydrogen atoms. In addition, several signals appeared in the aliphatic region (δ 0.80–3.24 ppm), consistent with a triterpenoid group. The ^{13}C NMR spectrum further supported this structural assignment, displaying deshielded carbon signals between δ 169 and 188 ppm, corresponding to carbonyl functionalities such as a carboxylic acid and a ketone. Signals observed in the range of δ 76–78 ppm were attributed to oxygenated sp^3 hybridized carbons, consistent with a hydroxylated carbon center in Figure 1. Taken together, the spectral data revealed the presence of a carboxylic acid group at the C-30 position, a hydroxyl group at C-3 in the β-orientation, a ketone function at C-11, and a double bond between C-12 and C-13.

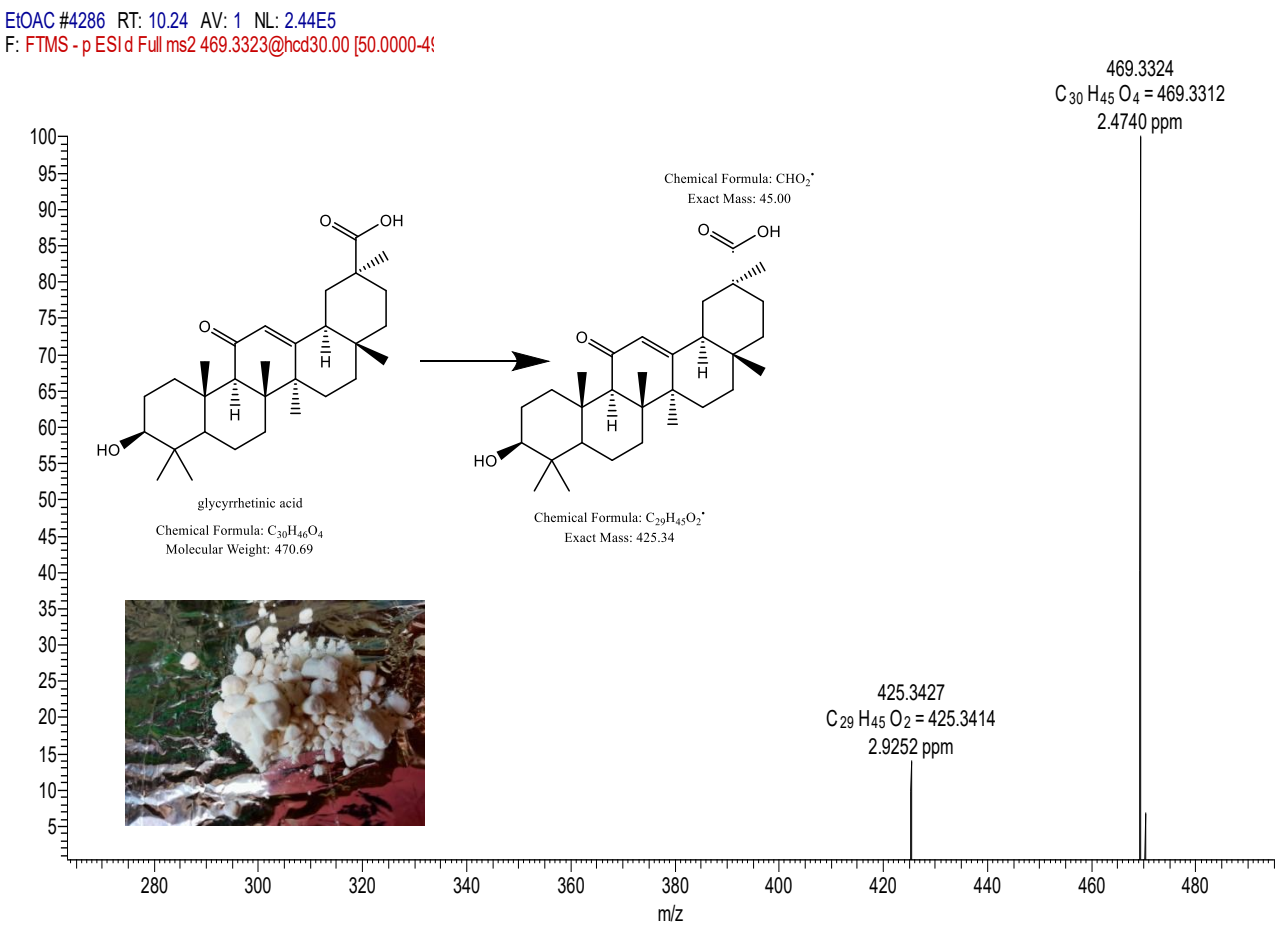


Figure 1. LC-MSMS fragmented pattern of the glycyrrhetinic acid in negative ionization mode.

3.3. HPLC-ESI-MS^n and UPLC-HRMS for Liquorice roots.

LC–HRMS analysis enabled the annotation of **62 metabolites** in Liquorice extracts, spanning phenolic acids, amino acids, flavonoids, flavonoid glycosides, chalcones, and triterpene saponins (Table 3 and Figure 2). Early-eluting compounds (RT 3-5 min) were assigned to small phenolic acids and amino acids, including catechol, gallic acid, caffeic acid, 6,7-dihydroxycoumarin, and tryptophan. Accurate mass measurements were within ±4 ppm. MS/MS spectra showed characteristic fragment ions: caffeic acid yielded m/z 135 and 107, gallic acid showed m/z 125 and 151, and tryptophan produced a base peak at m/z 159, consistent with indole ring cleavage. The compounds eluting between RT (7-10 min) was included isoflavones (genistin, glycitein, biochanin A, and genistein), flavones (apigenin-7-lactate, and chrysin), and chalcones (pallidiflorin, licochalcone A, iso-liquiritigenin). Their MS/MS spectra were dominated by aglycone fragment ions (m/z 253-269) and neutral losses of sugar moieties (162 Da). Genistin ([M-H]$^-$, m/z 431.0979) produced a fragment at m/z 269 corresponding to the genistein aglycone. Iso-liquiritigenin yielded a diagnostic fragment at m/z 255. The RT Between (15–30 min), several glycosylated flavonoids were detected, including iso-liquiritin apioside (m/z 549), iso-liquiritin (m/z 417), ononin (m/z 429), glucoliquiritin apioside (m/z 711), liquiritin apioside (m/z 549), and liquiritin (m/z 417). MS/MS spectra showed sequential losses of apiose and glucose, with a consistent aglycone ion at m/z 255. C-glycosyl flavones such as shaftoside and vicenin-2 displayed diagnostic fragments at m/z 383 and 353, characteristic of cross-ring cleavages. Several compounds at RT between (26–33) min were assigned to liquorice glycoside isomers (A/C1/C2 and B/D1/D2), observed at [M-H]$^-$ m/z 725 or 695, with fragment ions at m/z 549 and 255. Licuroside (m/z 549) was also detected, producing aglycone fragments at m/z 255 and 134. Later-eluting compounds between (RT 30-42 min) were identified as triterpene saponins, including Liquorice saponins J2, A3, G2, H2, albiziasaponins, uralsaponins, and glycyrrhizin. These compounds exhibited high-mass precursor ions (m/z 823–1011) and characteristic fragments at m/z 351, 193, and 113. Glycyrrhizin was identified at RT 37.7 min ([M-H]$^-$ m/z 821.4249, mass error 3.65 ppm). Glycyrrhetinic acid was also detected at RT 10.24 min ([M-H]$^-$ m/z 469). A late-eluting peak at RT 62.8 min was annotated as glucoliquiritin apioside ([M-H]$^-$ m/z 711.2133). Its MS/MS spectrum showed fragments at m/z 583, 549, 323, and 255, corresponding to stepwise sugar losses and the liquiritigenin aglycone.

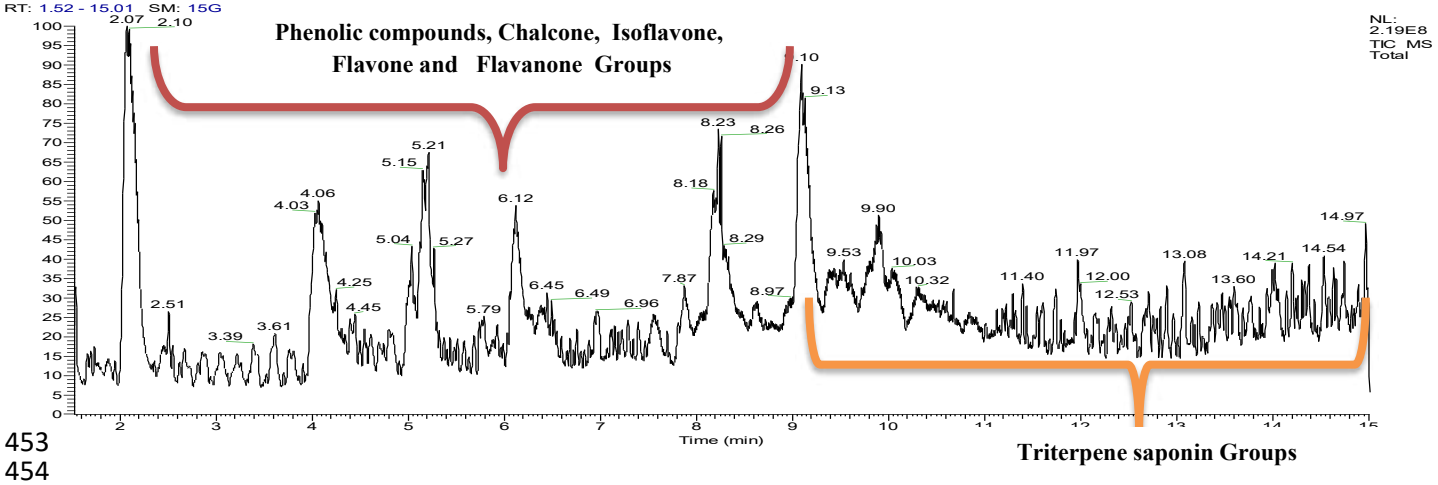


Figure 2: TIC of EtOAc fraction of Liquorice

Table 3: Secondary metabolites in *Glycyrrhiza glabra* roots were identified using two complementary analytical platforms: HPLC-ESI-MS^n and UPLC-HESI-MS/MS.

No	RT [Min] ESI-MS^n/ HRMS	*metabolite identification*	Chemical formula	HRMS/ negative ion mode ESI(-)			ESI-MS^n / Fragmentation in		Ref.
				Fragmentations Ions	Measured & calculated	Mass accuracy (ppm)	negative ion mode ESI(-)	positive ion mode ESI(+)	
Phenolic compounds and amino acids Groups									
1	-/3.52	*Catechol*	$C_6H_5O_2$	65.0381	109.0280, 109.0284	-3.8644	-	-	[48]
2	-/4.16	*trans-Caffeic acid*	$C_9H_8O_4$	135.0445, 107.0482	179.0338, 179.0339	-0.5711	-	-	MS-Dial
3	-/4.21	*6,7-Dihydroxycoumarin*	C_9H_6O4	133.0281, 105.0331	177.0182, 177.0182	-0.0051	-	-	MS-Dial
4	-/4.23	*Gallic acid*	$C_7H_6O_5$	151.0022, 125.0230	169.0132, 169.0131	0.0197	-	-	[48]
5	-/4.31	*Tryptophan*	$C_{12}H_{12}O_3$	159.0803	203.0704, 203.0703	0.5814	-	-	MS-Dial
6	-/5.54	*Hydroxy-methylglutaric acid*	$C_{10}H_{10}O_2$	119.0487, 73.0278	161.0595, 161.0597	-1.0324	-	-	MS-Dial
7	-/5.25	*trans-Ferulic acid*	$C_{10}H_{10}O_4$	178.0259, 149.0594, 134.0357	193.0493, 193.0495	-0.9756	-	-	MS-Dial
8	-/5.27	*Apigenin-7-lactate*	$C_{18}H_{14}O_7$	311.0563, 283.0599, 269.0448	431.0663, 431.0656	2.1565	-	-	MS-Dial
Chalcone, Isoflavone, Flavone and Flavanone Groups									
9	-/6.97	*Genistin*	$C_{21}H_{20}O_{10}$	370.0005, 269.0808, 250.0097, 89.0227	431.0979, 431.0973	1.5257	-	-	[49]
10	-/7.55	*Pallidiflorin*	$C_{16}H_{12}O_4$	252.0422, 239.0345, 141.1164	267.0652, 267.0656	-0.1135	-	-	Knapsack
11	-/7.80	*Biochanin A*	$C_{16}H_{12}O_5$	268.0376, 253.0507, 196.0527, 171.0440, 148.0152	283.0609, 283.0601	2.6571	-	-	Knapsack
12	-/7.62	*Glycitein*	$C_{16}H_{11}O_5$	268.0377, 253.0507, 223.0392, 195.0447, 171.0440, 148.0153, 135.0076	283.0609, 283.0601	2.6571	-	-	[49]
13	-/7.90	*Genistein*	$C_{15}H_{10}O_5$	241.0499, 197.0594, 133.0279, 93.0322	269.0455, 269.0444	3.7961	-	-	[49]
14	-/8.23	*Iso-liquiritigenin*	$C_{15}H_{12}O_4$	119.0487, 91.0173	255.0661, 255.0652	3.4108	-	-	[50]
15	-/8.42	*Chrysin*	$C_{15}H_{10}O_4$	191.0706, 135.0075	253.0504, 253.0495	3.2958	-	-	Knapsack
16	-/10.11	*Licochalcone A*	$C_{21}H_{21}O_4$	201.0914, 187.0755 $[M\text{-}H\text{-}A\text{-}CO\text{-}CH_3O]^-$	337.1445, 337.1434	3.1592	-	-	[50]
17	15.5/6.89	*Iso-liquiritin apioside*	$C_{26}H_{30}O_{13}$	492.1078, 255.0660, 173.9929, 135.0070	549.1611, 549.1603	1.5761	549, 255, 134, 296, 429	551, 419, 256, 136	[51]

18	15.9/6.20/ 5.31	*Shaftoside*	$C_{26}H_{28}O_{14}$	503.1194, 383.0772, 353.0668	563.1397, 563.1395	0.3155	563, 545, 503, 443, 353, 383, 354, 83	565, 562, 547, 433, 456, 346	[52]
19	21.7/ 7.34	*Iso-Liquiritin*	$C_{21}H_{22}O_9$	297.0661, 153.0182, 135.0074	417.1182, 417.1180	0.4458	417, 255, 135	419, 257, 238, 137, 154	[51]
20	16.1/3.16	*Ononin*	$C_{22}H_{22}O_9$	341.1071	429.1191, 429.1195	0.9321	429, 255, 135, 90, 296	-	[52]
21	16.2/5.95	*Glucoliquiritin apioside*	$C_{32}H_{40}O_{18}$	549.1613, 429.1087, 255.0661, 135.0077	711.2229, 711.2220	-1.3033	711 , 549, 255, 218	-	[53]
22	17.9/5.19	*Vicenin-2*	$C_{27}H_{30}O_{15}$	473.1076, 383.0777, 353.0671	593.1542, 593.1567	3.3718	593, 474, 441, 383, 354	595, 577, 529, 457, 427, 409, 379, 324	[52, 53]
23	20.1/5.93	*Iso-violanthin*	$C_{27}H_{30}O_{14}$	457.1145, 413.0859, 383.0761, 353.0668, 283.0603	577.1614, 577.1617	0.5197	577, 559, 457, 383, 364	-	[52]
24	20.8/5.19	*violanthin*	$C_{27}H_{30}O_{14}$	503.1194, 457.1127, 413.0845, 383.0775, 353.0665	577.1602, 577.1611	1.5593	577, 559, 503, 457, 382, 352, 296, 190	579, 525, 507, 489, 459, 427, 375, 188	[53]
25	20.8	*liquiritin apioside*	$C_{26}H_{30}O_{13}$	429.1049, 297.0766, 255.0661, 191.0342, 135.0072	549.1614, 549.1603	2.0207	549, 429, 255, 134, 91, 297	-	[53]
26	5.74	*Chalconaringenin-4-O-glucoside*	$C_{21}H_{22}O_{10}$	364.0956, 271.0612, 151.0023	433.1122, 433.1129	-1.7804	-	-	[53]
27	26.6/7.91	*Liquorice glycoside A/C1/C2 or isomer*	$C_{36}H_{38}O_{16}$	549.1594, 255.0661, 175.0392	725.2269, 725.2271	0.2757	725, 459, 255, 211	-	[52]
28	27/8.08	*Liquorice glycoside A/C1/C2 or isomer*	$C_{36}H_{38}O_{16}$	459.1630, 279.0772, 255.0662, 223.0607, 175.0390	725.2269, 725.2271	0.2757	725, 549, 255, 202	-	[52]
29	27.2/8.22	*Liquorice glycoside A/ C1/ C2 or isomer*	$C_{36}H_{38}O_{16}$	549.1064, 429.1064, 255.0061, 175.0391, 135.0074	725.2269, 725.2271	0.2757	725, 549, 255, 429	551, 419, 256, 238, 136, 81	[52]
30	28.1/8.28	*Licuroside*	$C_{26}H_{29}O_{13}$	255.0661, 135.0075	549.1599, 549.1603	-0.6467	549, 254, 218, 134	-	[51]
31	28.7/8.65	*Liquorice glycoside A/C1/C2 or isomar*	$C_{36}H_{38}O_{16}$	549.1625, 255.0662	725.2211, 725.2210	-0.1378	725, 695, 512, 399, 255, 209, 549	-	[52]
32	29.2/6.62	*liquiritin*	$C_{21}H_{22}O_9$	255.0661, 135.0074	417.2280, 417.2272	1.9201	417, 255, 135	419, 257, 238, 137	[53]
33	29.3/7.07	*Liquorice glycoside B/D1/D2*	$C_{35}H_{36}O_{15}$	549.1625, 531.1503, 399.1065, 255.0662, 145.0282	695.1113, 695.1117	0.5754	695, 549, 296, 255	697, 441, 260, 214, 196	[52]
34	33.1/6.48	*Liquorice glycoside B/D1/D2*	$C_{35}H_{36}O_{15}$	351.1495, 255.0659	695.2163, 695.2160	-0.4315	695, 549, 254, 218	-	[52]
35	31.9/8.80	*Liquorice glycoside A/ C1/ C2*	$C_{36}H_{38}O_{16}$	549.1614, 350.3724, 255.0657[$C_{15}H_{11}O_4$], 175.0392, 135.0077, 64.9919	725.2269, 725.2271	0.2757	725, 549, 531, 255	727, 709, 678, 357, 291	[52]
36	32.6/7.97	*Liquorice glycoside B/D1/D2*	$C_{35}H_{36}O_{15}$	531.1495, 255.0662	695.2172, 695.2180	1.1507	695, 549, 255	697, 535, 335, 299, 145, 178, 119	[52]
37	62.8/11.15	*Glucoliquiritin aposide or isomer*	$C_{32}H_{40}O_{18}$	549.1616, 285.9402, 255.0652	711.2133, 711.2138	0.7030	711, 549, 323, 729, 583	713, 657, 603, 537, 333	[52]
38	67.1	*Liquorice glycoside B/D1/D2*	$C_{35}H_{36}O_{15}$	549.1632, 255.0661	695.1111, 695.1118	1.007	695, 549, 255	-	[52]
Triterpene saponin Groups									
39	30.3/ 9.47	*Liquorice saponin J2/Uralsaponin C*	$C_{42}H_{64}O_{16}$	351.0564	823.4434, 823.4449	1.8216	823, 791, 350, 192, 112	-	[52]
40	29.6/11.28	*Liquorice saponin J2/Uralsaponin C*	$C_{42}H_{64}O_{16}$	351.0569, 323.1292, 223.0603	823.4110, 823.4111	0.1214	823, 351, 192, 174	-	[52]
41	30.6/8.93	*Liquorice saponin A3 or isomer*	$C_{48}H_{72}O_{21}$	821.4158, 459.1624, 573.4298, 403.1858, 351.0561, 193.047	983.5046, 983.5056	1.0167	983, 821, 803, 351	-	[51]
42	31.1/9.27	*Yunganoside K1 or isomer*	$C_{48}H_{72}O_{21}$	821.4240, 594.5227, 497.1123, 351.0561, 339.0911	983.5299, 983.5289	-1.0167	983, 821, 350	985, 453, 435, 389, 319, 240, 174, 120	[53]
43	31.6/	*yunganoside K2*	$C_{42}H_{62}O_{17}$	485.3271, 351.0566, 289.0562, 193.0345,	837.4304, 837.4297	-0.8358	837, 351, 288, 192, 112	-	[53]

				113.0228					
44	32/8.87	*Albiziasaponin B or isomer*	$C_{48}H_{74}O_{18}$	497.1140	969.5560, 969.5561	-0.4315	969, 907, 864, 793, 497, 351	-	[52]
45	32.9/9.71	*24-hydroxyl-glycyrrhizin*	$C_{42}H_{62}O_{17}$	351.0567, 280.9596, 193.0343, 113.0227	837.4277, 837.4297	2.3882	837, 351, 288, 192, 130	-	[53]
46	33.6/7.59	*22-Acetoxyl-glycyrrhizin*	$C_{44}H_{64}O_{18}$	351.0572, 193.0340	879.4341, 879.4377	4.0935	879, 351, 192, 172, 130	-	
47	34.4/9.12	*Albiziasaponin B or isomer*	$C_{48}H_{74}O_{18}$	497.1163	969.5214, 969.5210	-0.4125	969, 807, 351, 266	-	[52]
48	35.1/9.88	*Liquorice saponin G2*	$C_{42}H_{62}O_{17}$	661.3712, 490.9352, 351.0570, 289.0569, 193.0345, 113.0228	837.4328, 837.4297	-3.7017	837, 775, 351, 192, 112	-	[51]
49	37/10.24	*glycyrrhetinic acid*	$C_{30}H_{46}O_4$	425.3432[$C_{29}H_{45}O_2$],	469.3324, 469.3312	2.4740	469, 425	471, 453,413, 236 ,286	[54]
50	36/10.40	*Isomer of Liquorice saponin G2*	$C_{42}H_{62}O_{17}$	661.3624, 488.3778, 351.0569 [$C_{12}H_{15}O_{12}$], 289.0570, 193.0343, 113.0229	837.4279, 837.4297	2.1494	837, 351, 288, 192, 112	839, 834, 487, 423, 188, 156, 84	[51]
51	36.1/10.57	*Macedenosin B*	$C_{42}H_{62}O_{17}$	418.1939, 351.0569 [$C_{12}H_{15}O_{12}$], 289.0562, 193.0344, 113.0229	837.4298, 837.4297	-0.1194	837, 351, 192, 112	839, 487, 842, 627, 488, 451, 442, 319, 235	[53]
52	36.5	*/ Macedenosin A or isomer*	$C_{42}H_{62}O_{17}$	351.0565 [$C_{12}H_{15}O_{12}$], 193.0342, 113.0230	837.4399, 837.4397	-0.2388	837, 351, 192, 112	-	[53]
53	37.7/8.84	*18-α-glycyrrhizin*	$C_{42}H_{62}O_{16}$	645.3840, 536.3412, 351.0570[$C_{12}H_{15}O_{12}$], 289.0565, 193.0343, 113.0229	821.4249, 821.4279	3.6521	821, 645, 351, 192, 112	-	[55]
54	38.1/10.20	*macedonoside C*	$C_{42}H_{62}O_{16}$	351.0572, 193.0339	821.4232, 821.4279	5.7217	821, 803, 469, 351	-	[52]
55	38.6/10.86	*Liquorice sponin D3*	$C_{50}H_{76}O_{21}$	497.1222 [$C_{29}H_{21}O_8$], 321.0835 [$C_{12}H_{17}O_{10}$], 113.0230 [$C_5H_5O_3$]	1011.5358, 1011.5383	2.4714	1011, 993, 497, 321	-	[56]
56	39/10.37	*Yunganoside L2*	$C_{42}H_{62}O_{16}$	351.0569 [$C_{12}H_{15}O_{12}$], 289.0550, 193.0344, 113.0229	821.4280, 821.4279	-0.1217	821, 803, 351, 192, 112	-	[52]
57	39.4/10.55	*Uralsaponin A*	$C_{42}H_{62}O_{16}$	489.3746, 351.0571, 289.0567, 193.0342, 113.0229	821.4281, 821.4279	-0.2434	821, 351, 298, 192, 156	-	[52]
58	39.7/8.48	*Apioglycyrrhizin*	$C_{41}H_{62}O_{14}$	627.36.43, 561.3840	777.4364, 777.4388	3.0870	777, 627, 425, 355	-	[52]
59	40.7/10.73	*Liquorice saponin H2*	$C_{42}H_{62}O_{16}$	645.3675, 351.0571, 289.0566, 193.0346, 157.0130, 113.0229	821.4247, 821.4279	3.8956	821, 803, 671, 645, 759, 351	-	[51]
60	41/7.88	*Albiziasaponin B or isomer*	$C_{47}H_{74}O_{18}$	497.1173, 351.0568	969.5239, 969.5249	1.0314	969, 951, 497, 436, 351, 338	-	[52]
61	41.8/7.32	*Albiziasaponin B or isomer*	$C_{47}H_{74}O_{18}$	497.1158, 351.0568	969.5239, 969.5272	3.4037	969, 497, 451, 338, 262	-	[52]
62	42/11.97	*Liquorice saponin K2*	$C_{42}H_{62}O_{16}$	351.0569, 289.0560, 193.0345, 157.0131, 113.0229	821.4257, 821.4279	2.6782	821, 803, 351, 192, 112	823, 611, 565, 547	[51]

 # Chemical formulas were determined based on accurate mass measurements from HESI-MS/MS, and fragmentation pathways were elucidated using ESI-MS^n data

3.4. Determination of the calibration curve of liquorice.

The calibration curve was constructed by plotting the absorbance of different solutions against their corresponding concentrations. Figure S2 shows a straight line in both medium, indicating excellent linearity within this concentration range. The correlation coefficient for this calibration curve was determined to be 0.998 in both medium (PBS 5.5 and PBS 7.4), confirming a strong linear relationship between concentration and absorbance. The absorbance wavelength was 272 in PBS 5.5 and 321.2 in PBS 7.4.

3.5. Preparation of liquorice NSs:

β-Cyclodextrin was selected as the polymer for nano-sponge preparation due to its high complexing ability and stability with crosslinking agents. Diphenyl carbonate (DPC) was chosen as the cross-linker in the nano-sponge formulation based on its low lineal photo-degradation and lack of skin irritation and sensitization.

3.6. Determination of Encapsulation efficiency and loading Capacity.

Table (1) presents the encapsulation efficiency (EE%) of all Liquorice nano-sponges formulations, which ranged from 98.93 ± 7.22 to 100.07 ± 3.68. The molar ratio (1:4) showed higher encapsulation efficiency than (1:1). Loading capacity (LC) was observed to be higher in L3 (4:1), followed by L2 (1:4) and L1 (1:1).

3.7. Physicochemical Characterization of Liquorice nano-sponges

Liquorice nano-sponges analysis confirmed nanosized vesicles, with particle sizes ranging from 200.6 ± 3.91 to 289.4 ± 4.83 nm (Table 1). The formulations exhibited low polydispersity index (PDI) values (0.505–0.618). Zeta potential measurements showed that the nano-sponges possessed highly negative ZP values, as presented in Table (1).

3.8. Selection of Optimized NSs Formulation

Based on EE%, LC%, VS, PDI, and ZP results, the 4:1 molar ratio of HP-β-CD to DPC was selected as optimal. Using the same ratio, NSs were prepared with Epi-βCD: DPC (4:1) for Liquorice EtOAc extract encapsulation (L4). The resulting formulation showed high EE%, nanosized vesicles, low PDI, and a suitable ZP value (Table 1).

3.9. Characterization of the Optimized Liquorice nano-sponges

TEM imaging (Figure 3) revealed spherical, homogenous NSs without visible drug crystals on their surfaces.

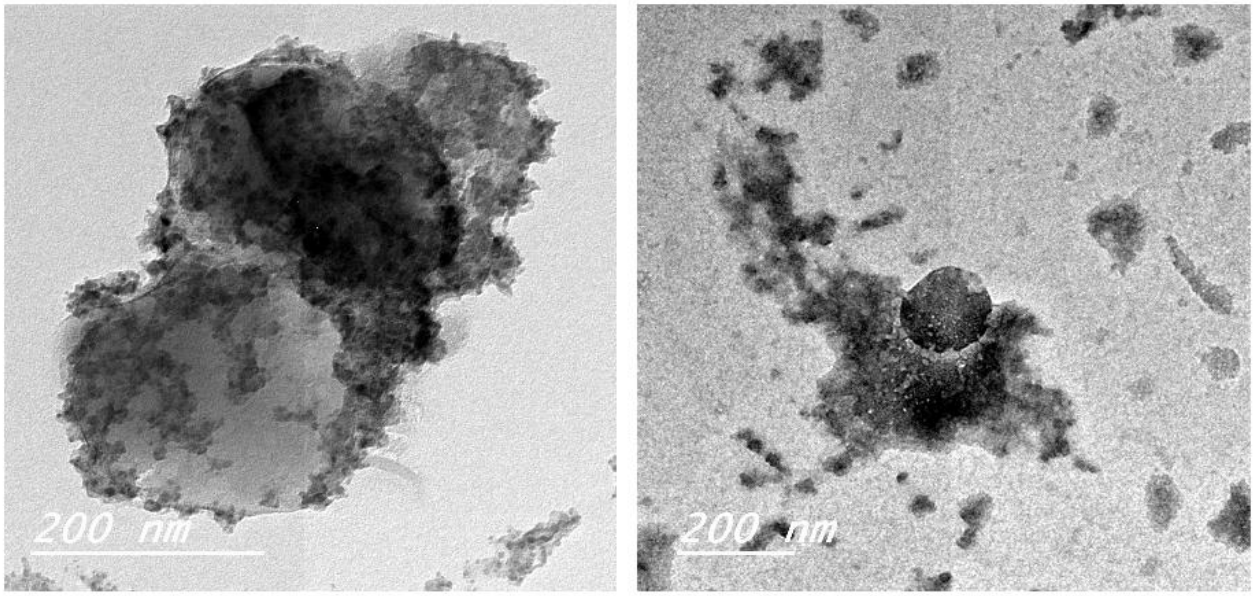
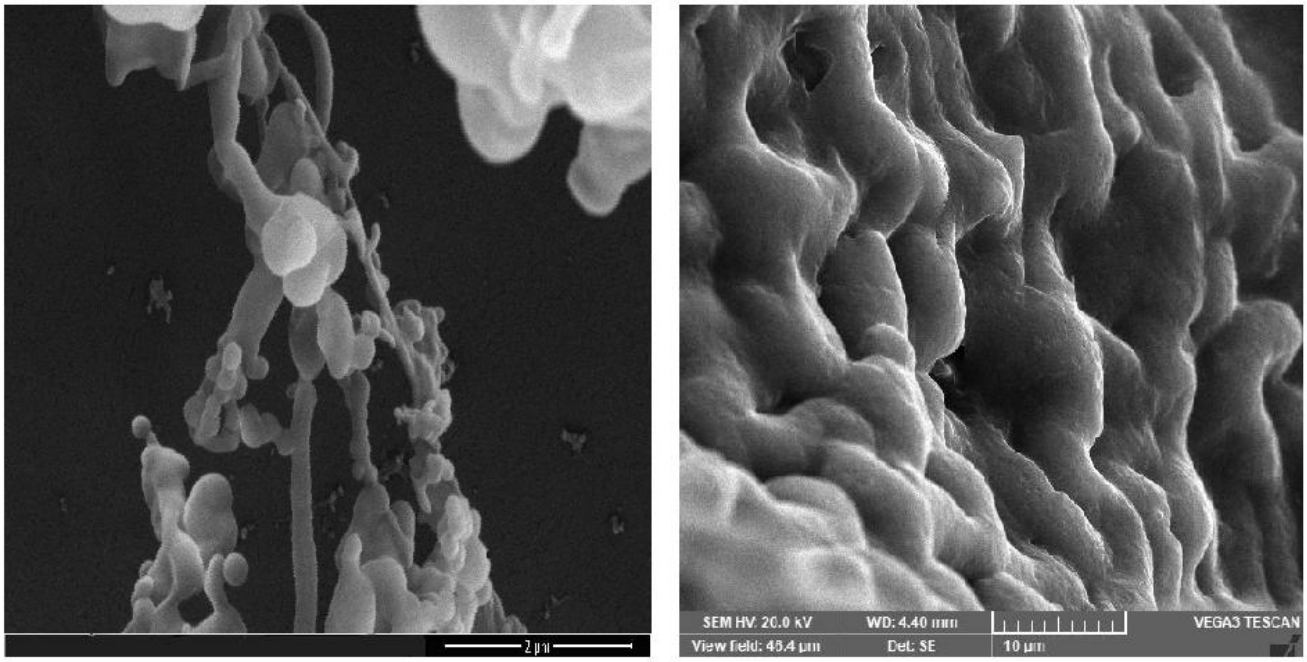


Figure 3: TEM micrographs of Nano-sponges optimized formulations of Liquorice EtOAc (a) and glycyrrhetinic acid (b)

Figure 4 presents the SEM micrographs of the developed NSs. The micrographs revealed nanosized, spherical particles with multiple surface pores. No residual drug crystals were observed, confirming complete encapsulation of the active compounds within the polymer matrix.



(a) (b)

Figure 4: SEM micrographs of Nano-sponges optimized formulations of Liquorice EtOAc (a) and glycyrrhetinic acid (b).

The FT-IR spectra of Liquorice EtOAc extract and glycyrrhetinic acid loaded NSs (L3 and L4) were compared to evaluate possible interactions between the glycyrrhetinic acid and excipients (Figure 5). HP-βCD displayed characteristic bands at 3415cm^{-1} (O-H stretching), 2929cm^{-1} (C-H stretching), 1645 cm^{-1} (H-O-H bending), 1157cm^{-1} (C-O stretching), and 1031cm^{-1} (C-O-C stretchin) DPC showed a distinctive absorption band at 1753 cm^{-1} corresponding to the carbonate bond.The spectrum of EPI-βCD exhibited peaks at 1288.36, 1249.79, and 721.33 cm^{-1}, along with CH_2-Cl wagging and C-Cl stretching bands. It also displayed OH, CH_2, and C–O–C stretching vibrations at ~3452.34, 3411.84, 3271.05, 2933.53, and 1099.35cm^{-1}. The liquorice EtOAc extract spectrum showed bands at 1372 and 1421 cm^{-1} (-CH bending), and at 2925.85cm^{-1} (-CH stretching), consistent with the presence of methyl and methylene groups in sugars, proteins, amino acids, and fatty acids. Additional signals were detected at 1040.78cm^{-1} (C–C stretching) and 1512.75cm^{-1} (C=C stretching of aromatic rings). The optimized NSs formulations EtOAc and glycyrrhetinic acid (L3 and L4) displayed shifts and broadening of characteristic peaks.

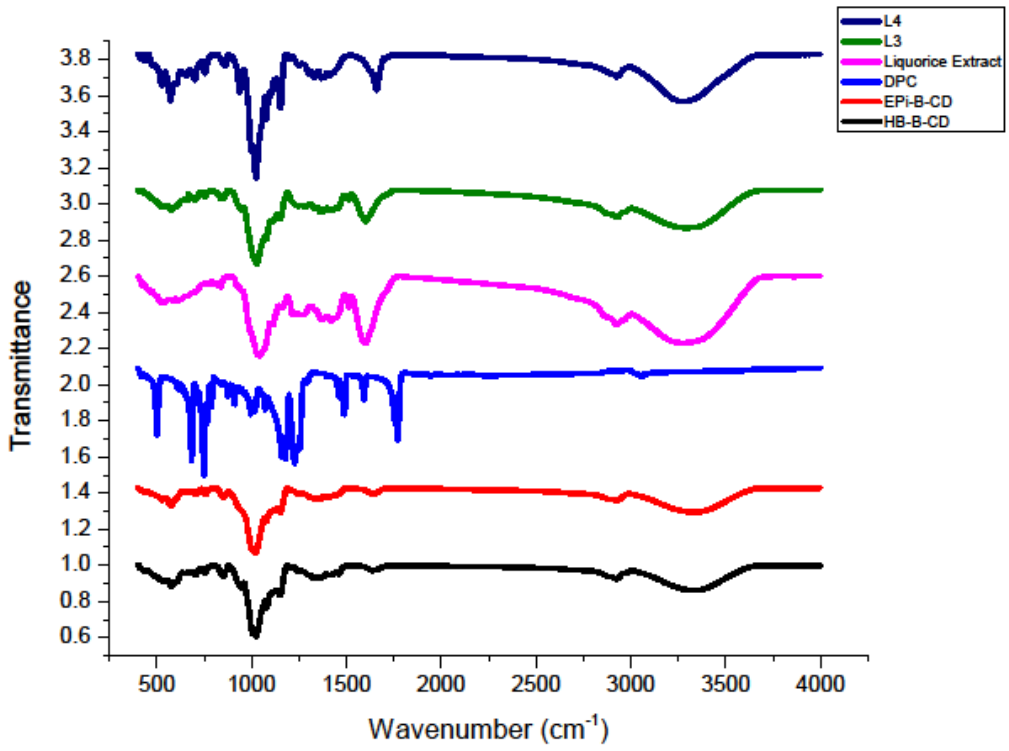


Figure 5: FT-IR spectra of nano-sponge components and optimized formulations, including *Liquorice* EtOAc-formulated nanosponges (L3), glycyrrhetinic acid-loaded nanosponges (L4), and *Liquorice* extract alone.

3.10. *In vitro* Release Study

The release behavior of Liquorice from the developed nano-sponges formulations in acidic and alkaline media is presented in Figure 6. In vitro release studies demonstrated a sustained drug release over 24 hours. The release profile followed a biphasic pattern, with an initial burst release followed by a slower, prolonged release phase. Release in alkaline medium was significantly higher than in acidic medium ($p \leq 0.05$). Mathematical modeling of the release kinetics showed that the correlation coefficient (R^2) values were more consistent with Higuchi's model than with zero-order or first-order models ($R^2 = 0.7096–0.8758$). The calculated release exponent (n) values ranged from 0.1548 to 0.2541.

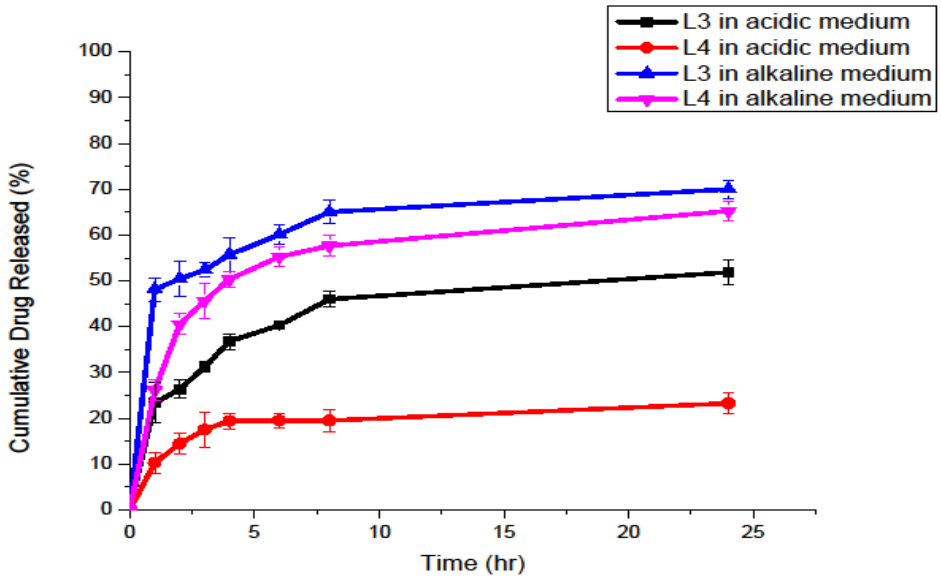


Figure 6: *In-vitro* release profiles of drugs from Nano-sponges optimized formulations (L3 and L4) at acidic medium (PBS 5.5) and alkaline medium (PBS 7.4).

3.11. Antioxidant activity

The antioxidant potential of the total extract, fractions, and glycyrrhetinic acid isolated compound was assessed by ABTS and DPPH assays, with vitamin C and Trolox as references standards. In the ABTS assay, vitamin C and glycyrrhetinic acid achieved complete inhibition at high concentrations, while the CH_2Cl_2, EtOAc, and BuOH fractions showed strong activity (>85%). At lower doses, EtOAc and BuOH retained substantial activity (62–78%), whereas glycyrrhetinic acid dropped markedly. The DPPH assay showed similar trends: vitamin C and Trolox gave the strongest dose dependent scavenging, while the total extract and EtOAc fraction maintained high inhibition (>75% at 50 µg/mL). CH_2Cl_2 and petroleum ether were weaker, and BuOH showed modest effects. Gly displayed concentration-dependent but consistently lower activity than the standards in Figure 7.

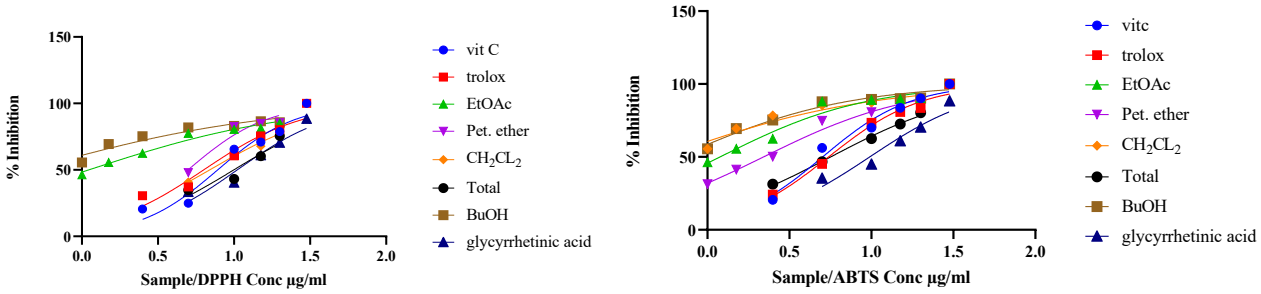


Figure 7: ***In vitro*** **DPPH· and ABTS⁺ antioxidant analysis of various extracts of the Liquorice.**

Both assays demonstrated that Liquorice extracts possess marked antioxidant activity, mainly concentrated in the phenolic-rich EtOAc and total extracts. Non-polar fractions (petroleum ether, CH_2Cl_2) showed weak efficacy, while BuOH was moderate. Glycyrrhetinic acid, though bioactive, contributed little compared to polyphenols. These findings confirm that

phenolic constituents are the main contributors to Liquorice antioxidant potential, consistent with previous reports. Among the tested fractions, the EtOAc extract exhibited the strongest and most consistent ABTS and DPPH radical-scavenging activity, comparable to the crude extract and superior to glycyrrhetinic acid alone in Figure 7.

3.12. *In vivo* Pharmacological study

Owing to its high antioxidant capacity and richness in phenolic compounds, the EtOAc fraction and glycyrrhetinic acid isolated compound were chosen for subsequent *in vivo* animal experiments. Furthermore, the dermal sensitivity test in the current study showed that all Liquorice preparations were safe when applied to skin, as they didn't cause any type of skin inflammation in the form of oedema or redness.

According to the results of the dermal sensitivity test, the efficacy study was performed. Liquorice preparations were applied topically on dorsal aspects of rats that were scratched by a sterilized needle tip (0.25 ml equivalent to 0.25 mg), and were instilled in both nostrils of each rat (each drop is 0.25 ml). In the current efficacy study, all rats assigned to the normal group and accommodated under the same conditions as the other groups, had their shaved dorsal skin intact and showed no signs of inflammation in their nostrils. Therefore, they received a zero score on macroscopic examination (0% of rats showed inflammation of the nose and skin = 100% curation) (Figures 8a & b & figures 9 &16).

Their measured inflammatory markers in serum were 601.9 ± 6.35 pg/ml for ICAM-1 (Figure 8c), 459.6 ± 27.98 pg/ml for IL-β4 (Figure 8d), and 926.7 ± 20.28 pg/ml for LTB-4 (Figure 8e). Histopathologic examination of their skin and nostrils also showed normal findings. The back skin consisted of an epidermis composed, from outside to inside, of the stratum corneum (black star) formed of keratin filaments, followed by the stratum granulosum, and then the stratum spinosum (yellow star) composed of irregular polygonal cells. The dermis was organized into two layers: the papillary layer (PL), characterized by fine collagen fibers and abundant blood vessels, and the deeper reticular layer (RL), formed of dense, thick collagen fibers (Figure 9). Examination of the nostrils revealed that the nasal cavity was lined with pseudostratified epithelium (PSE). The mucosa and submucosa contained numerous blood vessels (red arrows) along with mucin- and serous-secreting glands (Figure 16).

On the other hand, the rats assigned to the positive control group had their backs scratched with a sterilized needle tip, and their nostrils were instilled with capsaicin. They were then left untreated for the duration of the experiment. These rats showed unhealed skin and signs of inflammation in the form of redness, while their nostrils appeared edematous and red in four out of five rats. Macroscopic grading of the skin in four rats of this group was 3 (80% of rats suffered severe inflammation), while the fifth rat was scored 2 (20% of rats suffered moderate inflammation) (Figure 8a & figure 10). Nasal grading for all rats was 2 (100% of rats suffered inflammation of the nose) (Figure 8b & figure 17), as all exhibited edema and redness, and one rat additionally showed hemorrhagic spots around the nostrils. This macroscopic grading was significantly higher than that of the normal group.

Their ICAM-1, IL-β4, and LTB-4 levels were significantly higher than those of the normal and all treated groups, being 4631 ± 156.9, 3125 ± 13.81, and 3943 ± 41.05 pg/ml, respectively (Figures 8c, d & e). Histopathologic examination confirmed the biochemical assay results, as dermal tissue examination revealed that the epidermis had mainly lost the stratum corneum (red star) and stratum granulosum, while the stratum spinosum (yellow star) contained many pyknotic polygonal cells (red arrows). The dermal layer showed edema (E) separating collagen fibers with

scattered inflammatory cell infiltration (Figure 10). Histopathologic examination of the nose showed that the nasal cavity was lined by pseudostratified epithelium (PSE*), displaying detachment or complete denudation of the epithelial lining with focal ulceration (black arrow) due to injury or inflammation, as well as goblet cell depletion and signs of epithelial cell degeneration and nuclear karyolysis (yellow arrows). Submucosal changes due to edema (E) and atrophy of submucosal glands (blue arrows) were also detected (Figure 17).

The results of treatment with Liquorice EtOAc extract, Liquorice EtOAc nano-sponge preparation, Liquorice glycyrrhetinic acid, Liquorice glycyrrhetinic acid functionalized nano-sponge, as well as the blank nano-preparation in the efficacy study, showed noticeable improvement in the appearance of both the dorsal skin and the nose upon macroscopic examination. Regarding the nasal curative effect, treatment with Liquorice EtOAc extract resulted in 3 out of 5 rats being scored 1, and 2 out of 5 rats being scored 0, corresponding to a nasal curative rate of 40%. In the groups treated with either Liquorice EtOAc nano-sponge or Liquorice glycyrrhetinic acid, 1 out of 5 rats was scored 1 and 4 out of 5 rats were scored 0, corresponding to a nasal curative rate of 80% for each treatment. In contrast, treatment with Liquorice glycyrrhetinic acid functionalized nano-sponge achieved a nasal curative rate of 100%, as all rats were graded 0. On the other hand, in the group treated with the blank preparation, only 1 out of 5 rats was graded 0, corresponding to a nasal curative rate of 20% (Figure 8a & figures 18-22).

Grading of dorsal skin healing revealed the following results: Rats treated with Liquorice EtOAc extract showed that 3 out of 5 rats were scored 2, and 2 out of 5 rats were scored 1, giving an initial dermal healing rate of 40%. In rats treated with Liquorice EtOAc nano-sponge preparation, 2 out of 5 rats were scored 2, and 3 out of 5 rats were scored 1, corresponding to an initial dermal healing rate of 60%. For the group treated with Liquorice glycyrrhetinic acid, all rats were scored 1, indicating an initial dermal healing rate of 100%. The best prognosis was observed in the group treated with Liquorice glycyrrhetinic acid functionalized nano-sponge, where 3 out of 5 r ats were scored 0 and 2 out of 5 were scored 1, indicating progression toward complete wound healing (complete dermal healing rate 60% and initial dermal healing rate 40%). The poorest macroscopic appearance among all treatments was observed in the group treated with the blank preparation, in which 1 rat was graded 1, 2 rats were graded 2, 1 rat was graded 3, and only 1 rat was graded 0 (complete dermal healing rate 20%, initial dermal healing rate 20%, and 20% uncured) (Figure 8b & figures 11-15).

Treatment with Liquorice preparations, as well as the blank nano-preparations, produced a significant reduction in the measured inflammatory biochemical parameters ICAM-1, IL-β4, and LTB-4 (Figures 8c, d & e) when compared to the positive control group. However, these results remained significantly higher than those of the normal group, except for the levels of LTB-4 in the EtOAc extract and glycyrrhetinic acid groups, which were not significantly different from the normal control group. It is noteworthy that the levels of ICAM-1 and IL-β4 in the Liquorice EtOAc nano-sponge group were significantly lower than those in the Liquorice EtOAc extract group. The levels of ICAM-1 in both the Liquorice glycyrrhetinic acid and glycyrrhetinic acid functionalized nano-sponge groups were significantly lower than in both Liquorice EtOAc groups. The levels of IL-β4 in both glycyrrhetinic acid groups were significantly higher than in the Liquorice EtOAc extract group; however, the IL-β4 level in the glycyrrhetinic acid functionalized nano-sponge group was significantly lower than that in the glycyrrhetinic acid group. The LTB-4 level in the glycyrrhetinic acid functionalized nano-sponge group was significantly higher than the levels observed in both the Liquorice EtOAc extract and Liquorice

glycyrrhetinic acid groups. The ICAM-1 level in the blank group was significantly higher than in the Liquorice glycyrrhetinic acid and glycyrrhetinic acid functionalized nano-sponge groups. However, the IL-β4 level in the blank group was significantly lower than that in the EtOAc extract group, but higher than in the Liquorice EtOAc nano-sponge, glycyrrhetinic acid, and glycyrrhetinic acid functionalized nano-sponge groups. The LTB-4 level in the blank group was significantly higher than in both Liquorice EtOAc groups and the glycyrrhetinic acid group. The ICAM-1 levels were 2805 ± 119.2, 1175 ± 58.76, 682.4 ± 8.25, 560.6 ± 15.35, and 1250 ± 80.74 pg/ml, respectively, for the five groups. The IL-β4 levels were 1944 ± 100.46, 948.7 ± 25.73, 819.6 ± 4.97, 500.4 ± 12.02, and 1668 ± 64 pg/ml, respectively, for the five groups. The LTB-4 levels were 1313 ± 191.9, 1535 ± 34, 1105 ± 66.77, 1846 ± 95.35, and 2227 ± 170.6 pg/ml, respectively, for the five groups.

Histopathologic Examination of the effects of treatment with Liquorice and the blank nano-preparations on dermal and nasal tissues were confirmed through histopathologic examination, which revealed the following findings: Examination of the dermal tissue from the Liquorice EtOAc extract group showed an epidermis with pyknotic polygonal cells in the stratum spinosum (red arrow). The dermis consisted of a papillary layer (PL) characterized by loose, destructured connective tissue and a deeper reticular layer (RL) formed of thick collagen fibers infiltrated with inflammatory cells (Figure 11). In contrast, the skin tissues of both the Liquorice EtOAc nano-sponge and Liquorice glycyrrhetinic acid groups appeared normal. The epidermis consisted, from outside to inside, of the stratum corneum (black star) composed of keratin filaments, the stratum granulosum in the middle, and the stratum spinosum (yellow star) formed of irregular polygonal cells. The dermis included a PL with loose fine collagen fibers and numerous blood vessels, and a deeper RL composed of thick collagen fibers (Figures 12 & 13).

The best dermal tissue architecture among all Liquorice treated groups was observed in the Liquorice glycyrrhetinic acid functionalized nano-sponge group. This group showed a normally structured epidermis with clearly defined stratum corneum, stratum granulosum, and stratum spinosum layers. The dermis appeared normal with minimal edema (E), composed of a PL and a deeper RL (Figure 14).

Additionally, the blank nano-sponge group exhibited a nearly normal skin structure. The epidermis consisted, from outside to inside, of a stratum corneum (black star) formed of keratin filaments, a stratum granulosum in between, and a stratum spinosum (yellow star) composed of irregular polygonal cells. The dermis was formed of a PL containing fine collagen fibers and frequent blood vessels, and a deeper RL with thick collagen fibers (Figure 15).

The nasal tissue of the Liquorice EtOAc extract group showed that the nasal cavity was lined by pseudostratified epithelium (PSE) which showed normal appearance , average number of goblet cells, and the lamina propria had minimal inflammatory cell infiltration (Orange arrows), mainly concentrated around blood vessels (Red arrow), with edematous foci (Figure 18). While, Liquorice EtOAc nano-sponge preparation group nasal tissue examination, showed that the nasal cavity was lined by pseudostratified epithelium (PSE) which showed normal appearance , average number of goblet cells and the lamina propria had minimal inflammatory cell infiltration (Orange arrows), with decreased edema (E) and average thickness and normal appearance of blood vessels (Red arrow) (Figure 19). The best histopathologic appearances of nasal tissues were those of Liquorice glycyrrhetinic acid and glycyrrhetinic acid functionalized nano-sponge groups which appeared as the normal nasal tissue, as the nasal cavities were lined by normal looking pseudostratified epithelium (PSE), average number of goblet cells and the lamina propria had no inflammatory cell infiltration, with minimal oedema in the tissues of the

Liquorice glycyrrhetinic acid group, while there was no oedema in the tissues of the Functionalized glycyrrhetinic acid group (E) and normal looking blood vessels (Red arrow) (Figures 20&21). The photomicrography of nasal tissue of blank group, showed that he nasal cavity was lined by pseudostratified epithelium
(PSE) which showed normal appearance and average number of goblet cells and the lamina propria had minimal inflammatory cell infiltration (Orange arrows) with decreased oedema (E) and vascular congestion (Fig 22).

Fig8A: Grading of the Curative Effect of Topical Liquorice on Nasal Inflammation

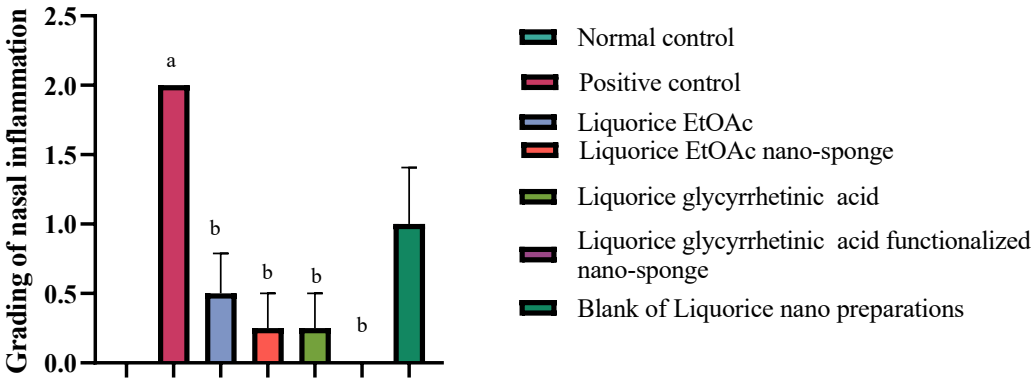


Fig8B: Grading of the Curative Effect of Topical Liquorice on Dorsal Skin Inflammation

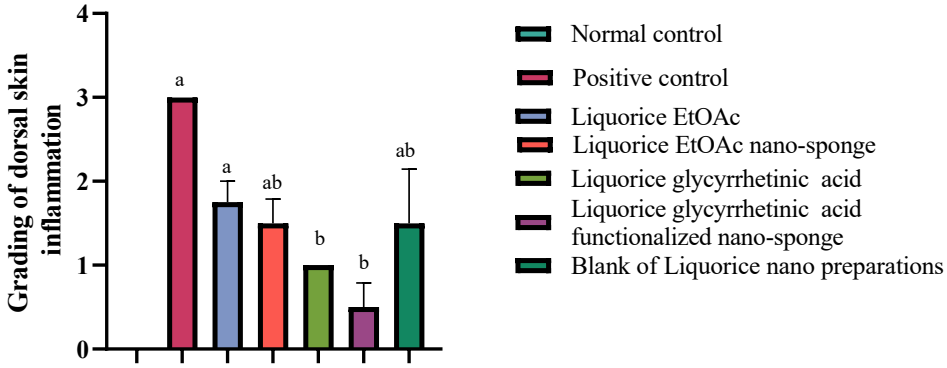


Fig 8C:Effect of Topical Liquorice on ICAM-1 in Inflammatory Skin Lesions

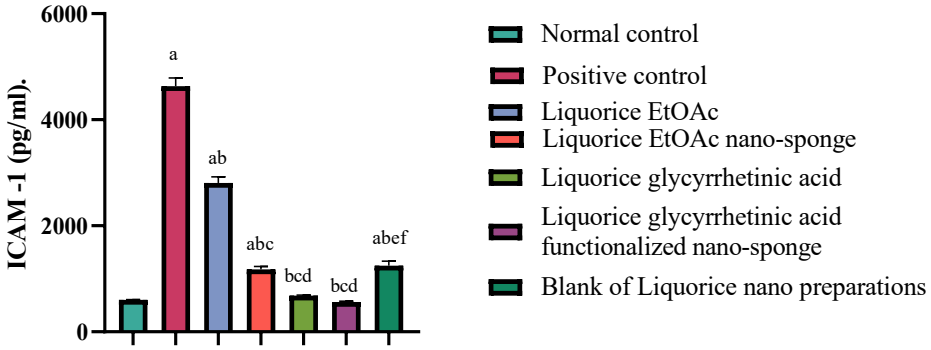


Fig 8D:Effect of Topical Liquorice on IL-β4 in Inflammatory Skin Lesions

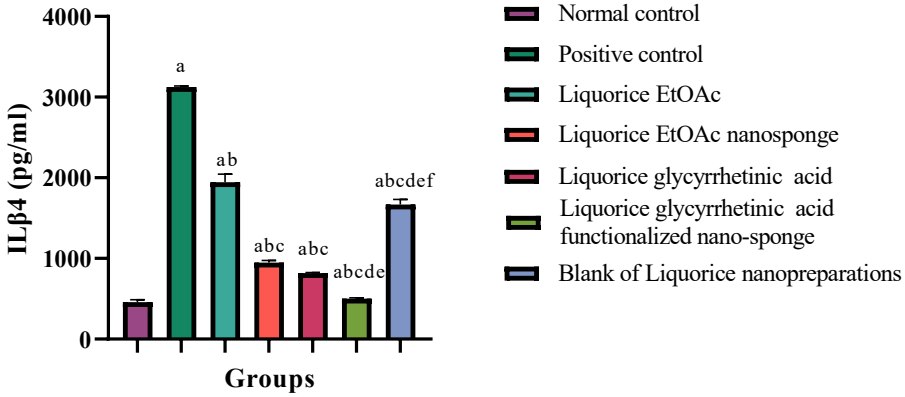
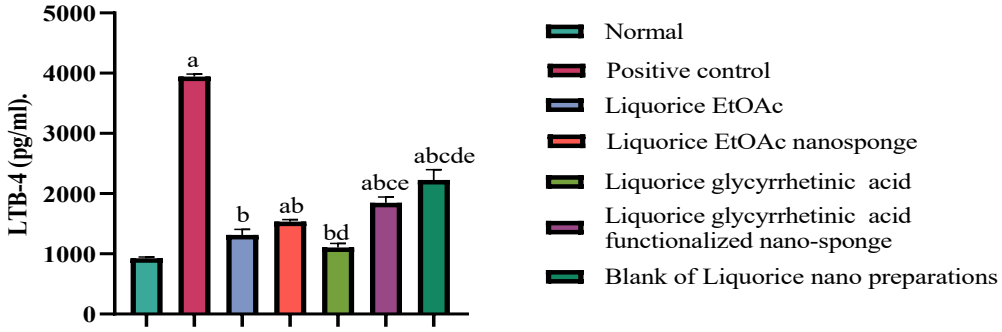


Fig 8E: Effect of Topical Liquorice on LTB-4 in Inflammatory Skin Lesions



Figures 8 A-E: Results were expressed as means of values ± standard error(SE). N=5. P value ≤ 0.001. (a) Significantly different from normal control group. (b) Significantly different from positive control (untreated) group. (c) Significantly different from Liquorice EtOAc extract group. (d) Significantly different from Liquorice EtOAc nano-sponge group. (e) Significantly different from Liquorice glycyrrhetinic acid group. (f) Significantly different from Liquorice glycyrrhetinic acid Functionalized nano-sponge group. The relation between the lengths of the columns and therapeutic effects are inversely proportionate.

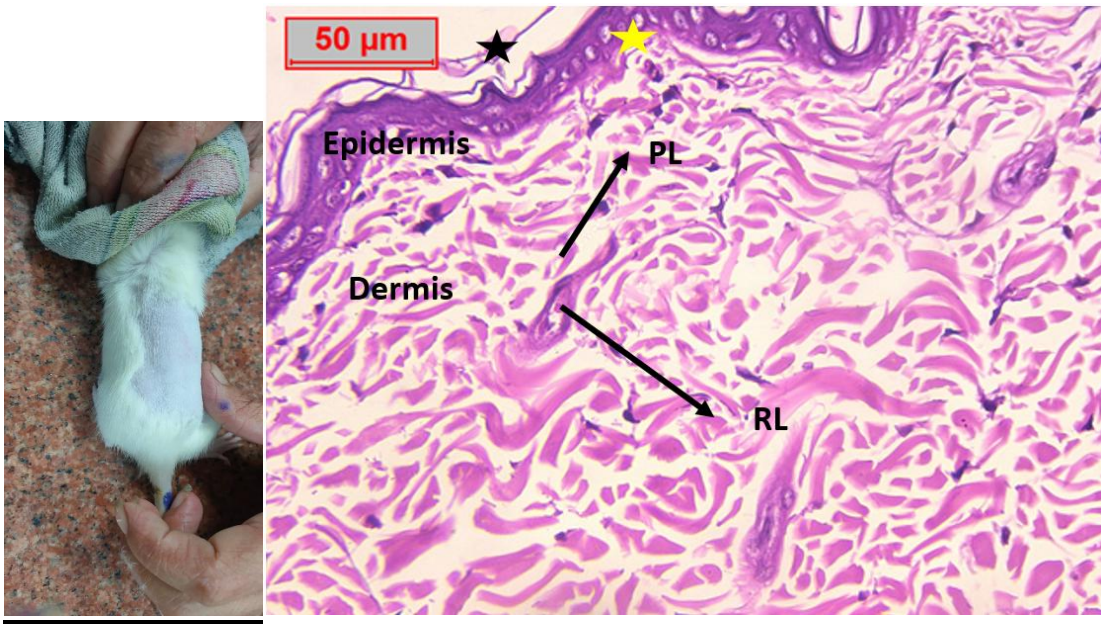


Figure 9: A normal photography of the skin of the **Normal group rat.** A photomicrography of normal skin tissue of skin tissue of the same group, formed of epidermis which consist from outside to inside: Stratum cornum (black star) formed of keratin filaments, stratum granulosa in between and then stratum spinosum (yellow star) formed of irregular polygonal cells. The Dermis layer; formed of papillary layer (PL) consist of loose finer collagen and frequent blood vessels; and deeper reticular dermal layer (RL) formed of thick collagen fibers (H&E 400x)

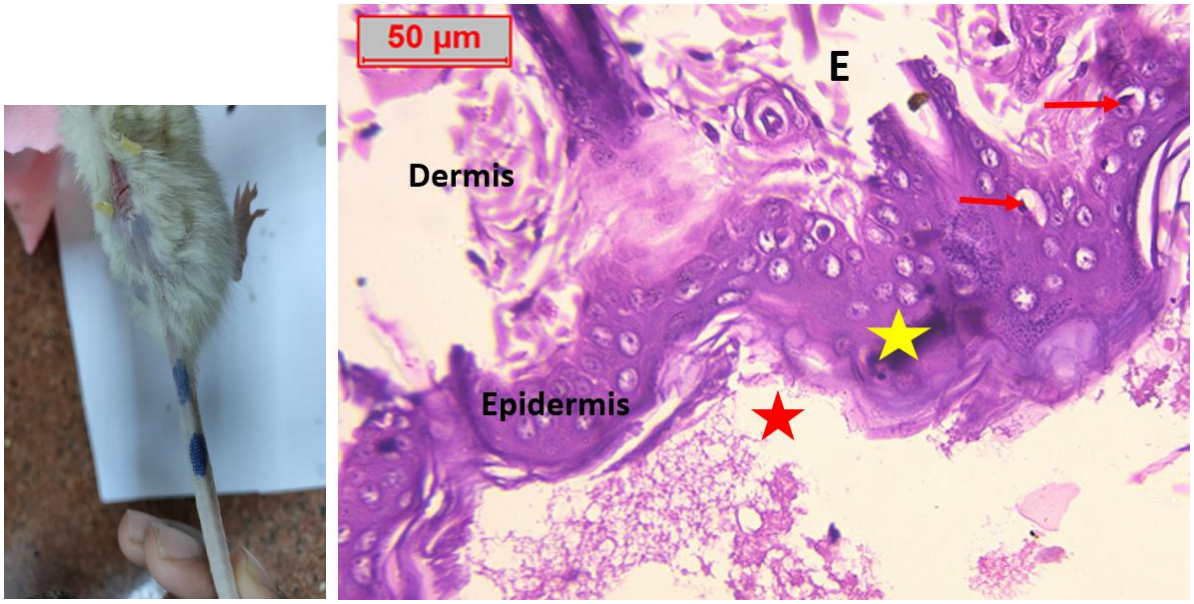


Figure 10: A photography of grade 3 scratch of skin of the dorsal aspect of a **Positive control** group rat. A photomicrography of skin tissue of the same group, shows that the epidermis mainly lost stratum cornum (Red star), stratum granulosa in between and then stratum spinosum (yellow star) have many of pyknotic polygonal cells (red arrows). The Dermis layer; show edema (E) separating collagen fiber with scattered inflammatory cells infiltrate (H&E 400x).

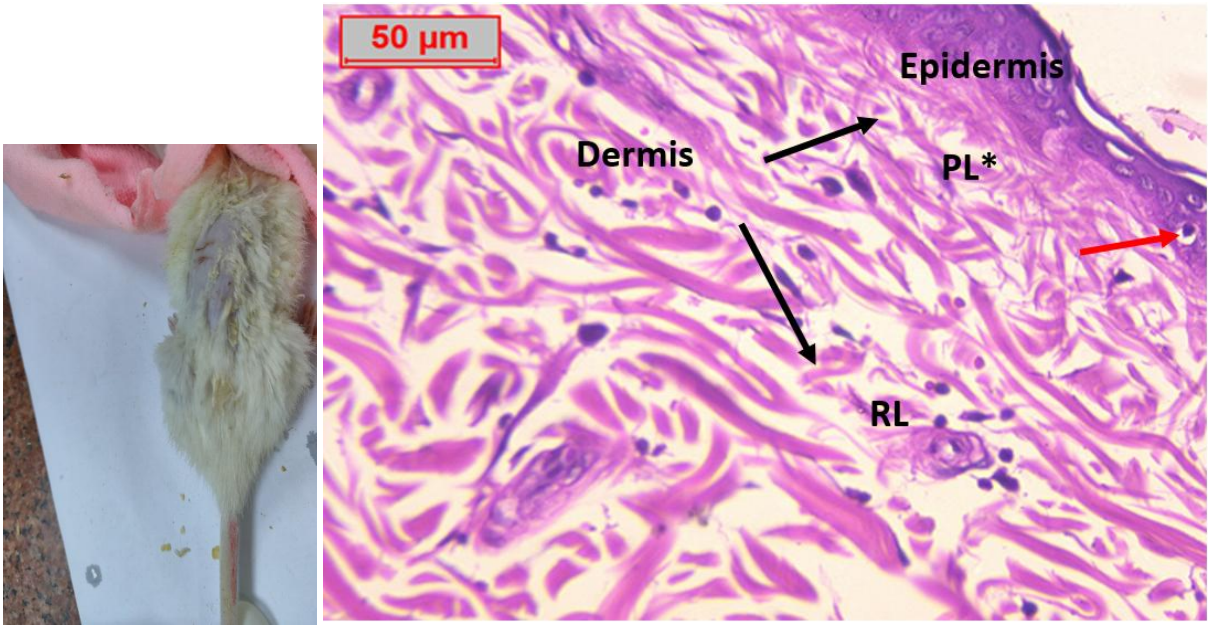


Figure 11: A photography of grade 2 scratch of skin of the dorsal aspect of **a Liquorice EtOAc extract group** rat. A photomicrography of skin tissue of the same group, formed of epidermis which show in stratum spinosum pyknotic polygonal cells (Red arrow). The Dermis layer; formed of papillary layer (PL) consist of loose desrtuctive; and deeper reticular dermal layer (RL) formed of thick collagen fibers with inflammatory cells infiltrate. (H&E 400x)

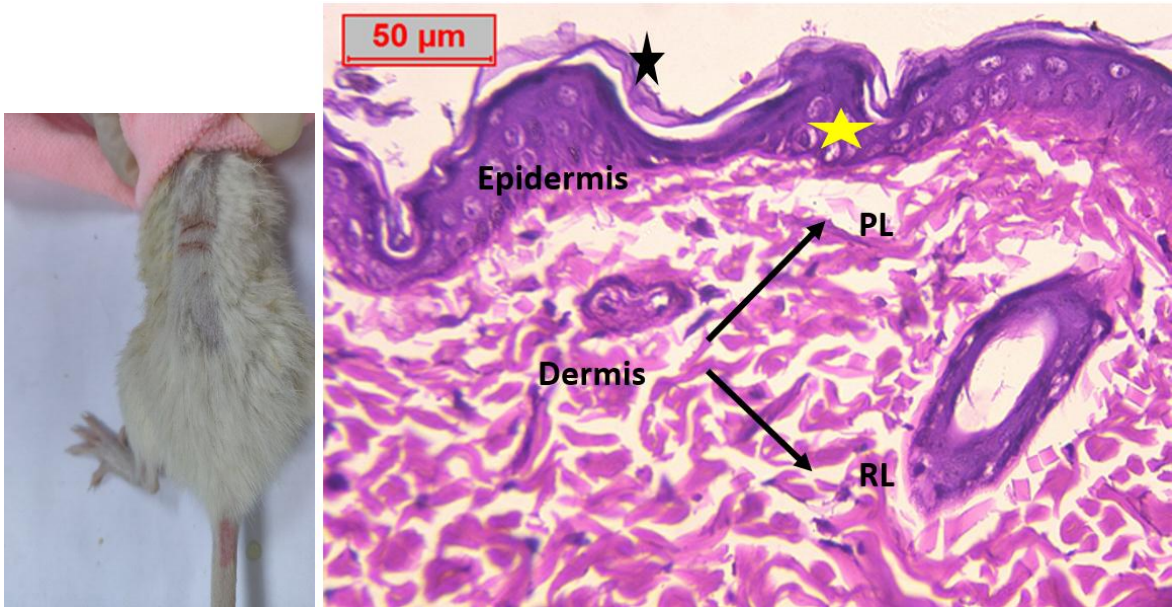


Figure 12: A photography of grade 2 scratch of skin of the dorsal aspect of **a Liquorice EtOAc nano-sponge group** rat. A photomicrography of skin tissue of the same group**,** formed of epidermis which consist from outside to inside: Stratum cornum (black star) formed of keratin filaments , stratum granulosa in between and then stratum spinosum (yellow star) formed of irregular polygonal cells . The Dermis layer ; formed of papillary layer (PL) consist of loose finer collagen and frequent blood vessels ; and deeper reticular dermal layer (RL) formed of thick collagen fibers . (H&E 400x)

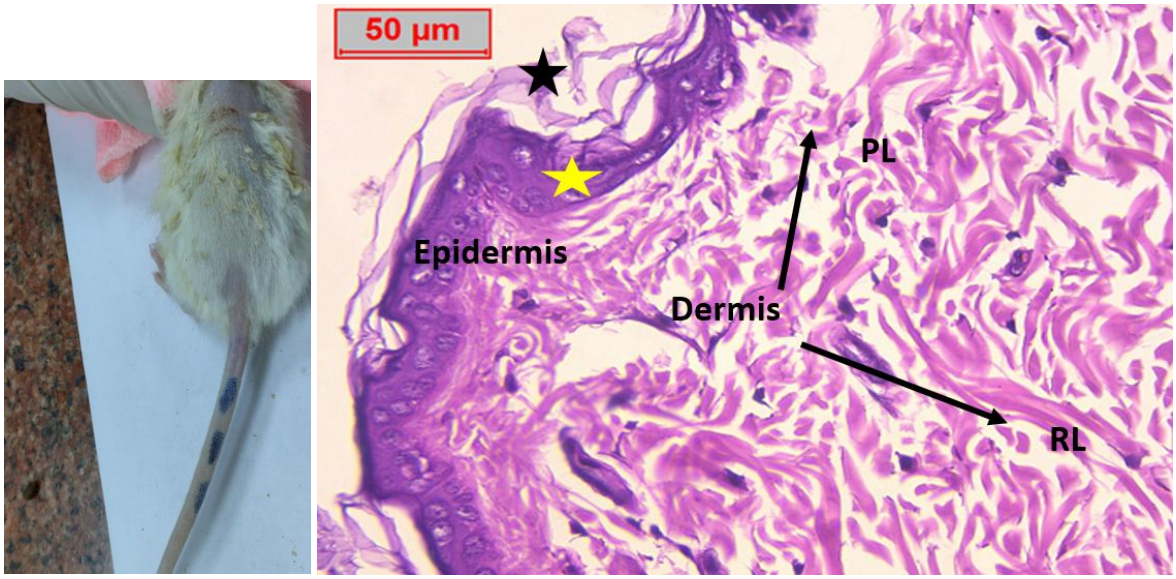


Figure 13: A photography of grade 1 scratch of skin of the dorsal aspect of **a Liquorice Glycyrrhetinic acid group** rat. A photomicrography of normal skin tissue of the same group**,** formed of epidermis which consist from outside to inside: Stratum cornum (black star) formed of keratin filaments , stratum granulosa in between and then stratum spinosum (yellow star) formed of irregular polygonal cells . The Dermis layer ; formed of papillary layer (PL) consist of loose finer collagen and frequent blood vessels ; and deeper reticular dermal layer (RL) formed of thick collagen fibers. (H&E 400x)

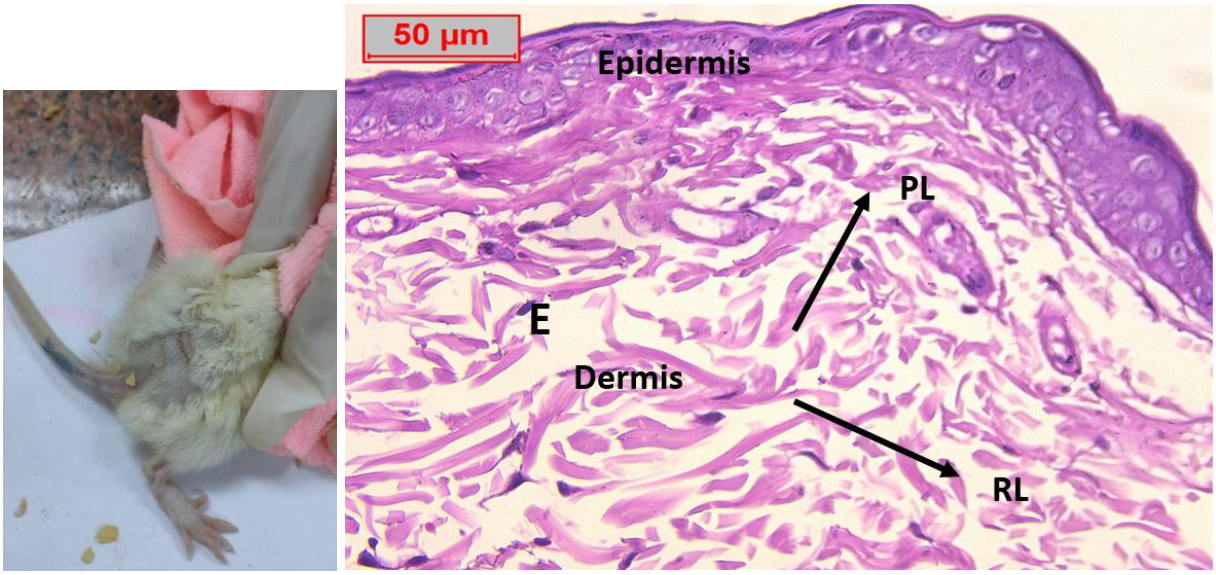


Figure 14: A photography of grade 0-1 scratch of skin of the dorsal aspect of **a Liquorice Glycyrrhetinic acid Functionalized nano-sponge group** rat. A photomicrography of normal skin tissue of the same group**,** formed of epidermis with normal appearance of Stratum cornum, stratum granulosa in between and then stratum spinosum. The Dermis layer normally looking with minimal edema (E); formed of papillary layer (PL); and deeper reticular dermal layer (RL). (H&E 400x)

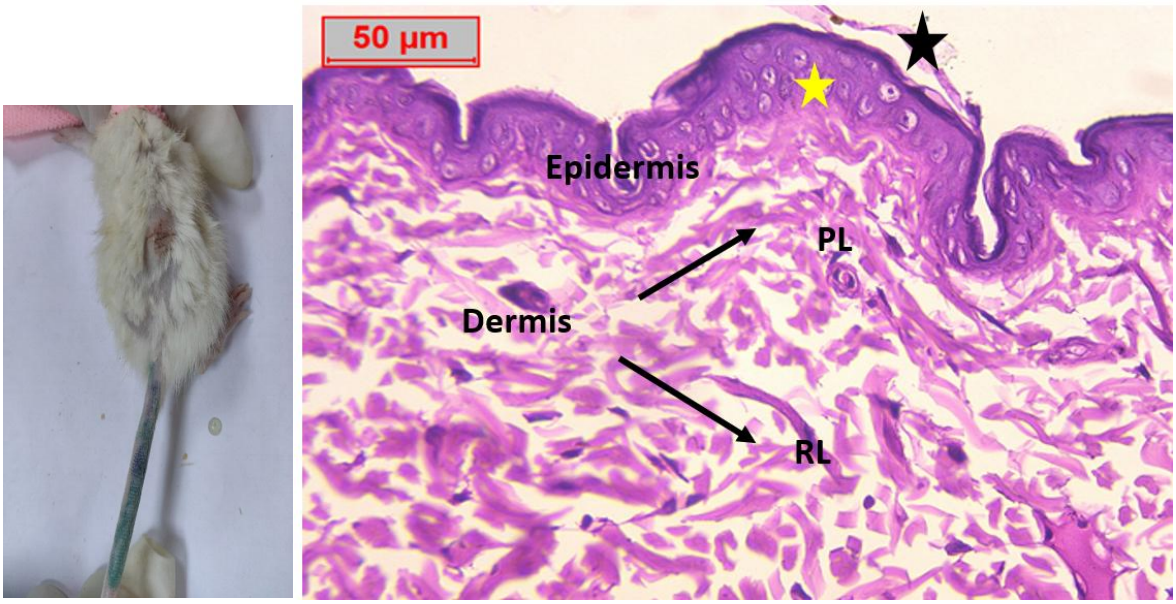


Figure 15: A photography of grade 2-3 skin scratch of the dorsal aspect of **Blank group** rat. A photomicrography of normal skin tissue of the same group, formed of epidermis which consist from outside to inside: Stratum cornum (black star) formed of keratin filaments, stratum granulosa in between and then stratum spinosum (yellow star) formed of irregular polygonal cells. The Dermis layer; formed of papillary layer (PL) consists of loose finer collagen and frequent blood vessels; and deeper reticular dermal layer (RL) formed of thick collagen fibers. (H&E 400x)

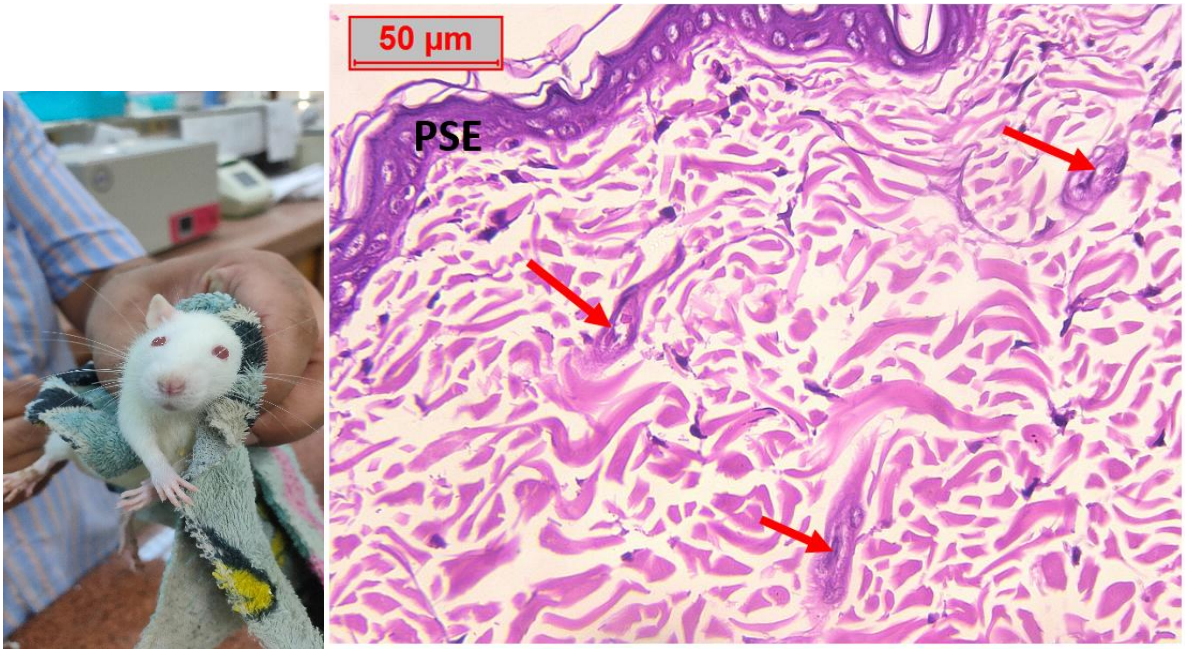


Figure 16: A normal photography of the nose of the **Normal group:** Photomicrography of nasal tissue of the same group, show that the nasal cavity is lined by pseudostratified epithelium (PSE) , mucosa and submucosa region filled of blood vessels (red arrows) , musin and serous secreting gland (H&E 400x).

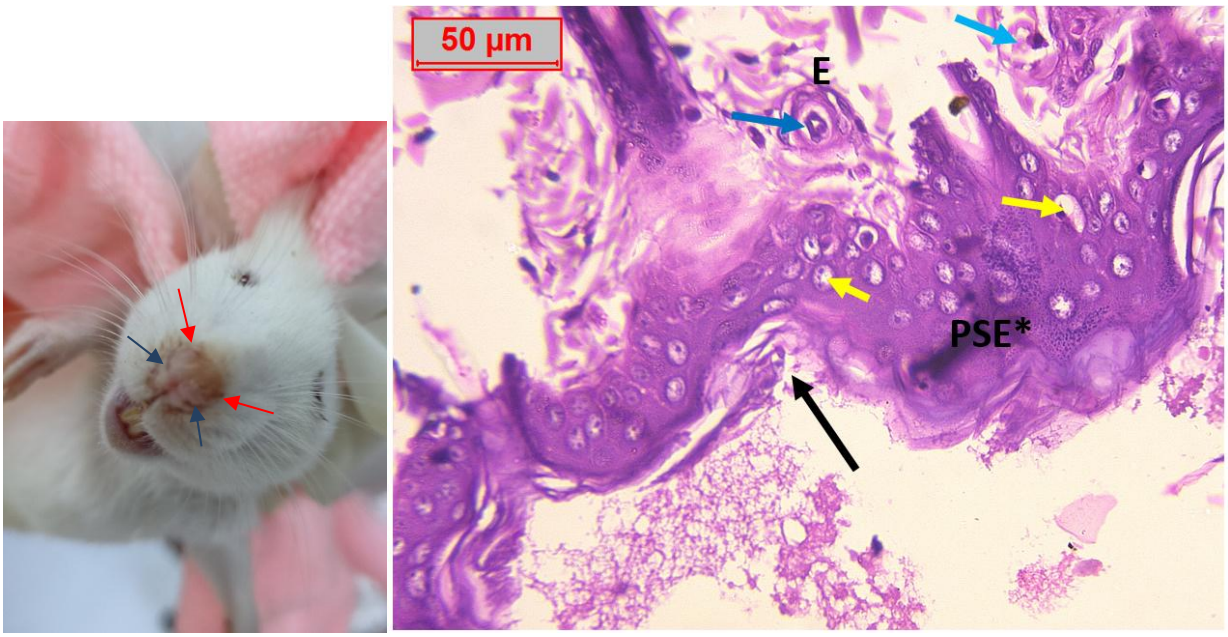


Figure 17: A photography of the nose **Positive control (Untreated) group**: Red arrows point to the hemorrhagic spots, blue arrows point to severe oedema of the skin of the nostrils markedly narrowing the nasal orifices. Photomicrography of nasal tissue of the same group, show that the nasal cavity is lined by pseudostratified epithelium (PSE*) showing detachment or complete denudation of the epithelial lining with focus of ulceration (Black arrow) due to injury or inflammation. Goblet cell depletion and signs of epithelial cells degeneration and nuclear Karyolysis (Yellow arrows). Submucosal Changes due to Edema (E) with atrophy of submucosal glands (Blue arrows). (H&E 400x)

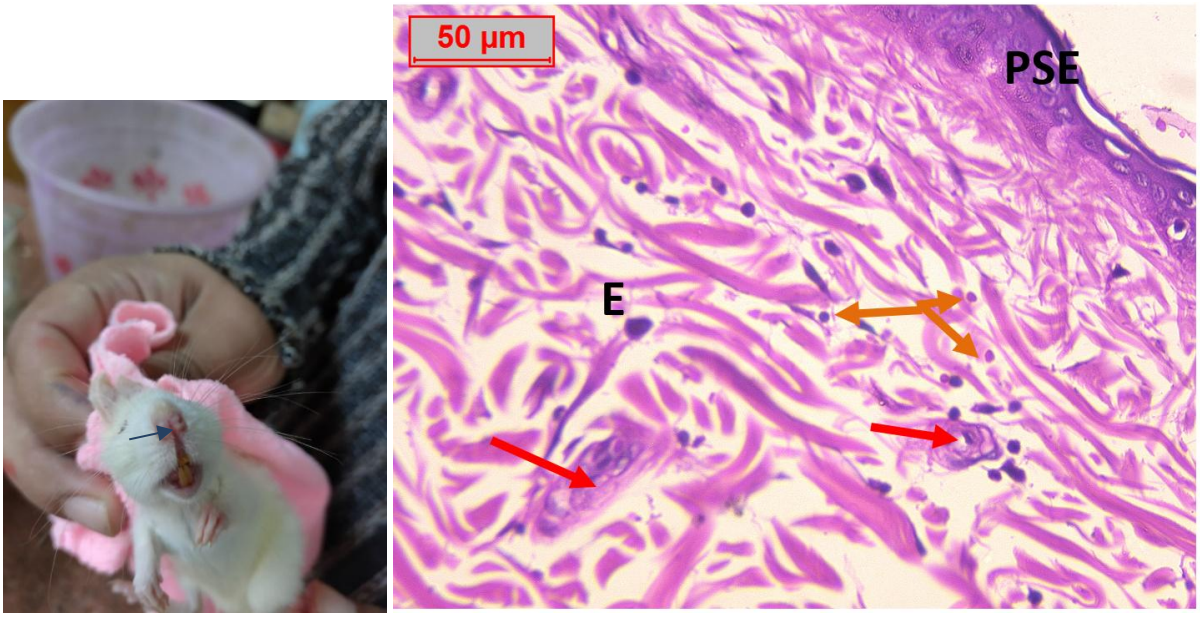


Figure 18: A photography of the nose of **Liquorice EtOAc extract group**: Blue arrow points to mild swelling of the skin surrounding the nasal orifice. Photomicrography of nasal tissue of the same group, shows that the nasal cavity is lined by pseudostratified epithelium (PSE) which showed normal appearance , average number of goblet cells , The lamina propria has minimal inflammatory cell infiltration (Orange arrows), mainly concentrated around blood vessels (Red arrow). with edematous foci(E). (H&E 400x)

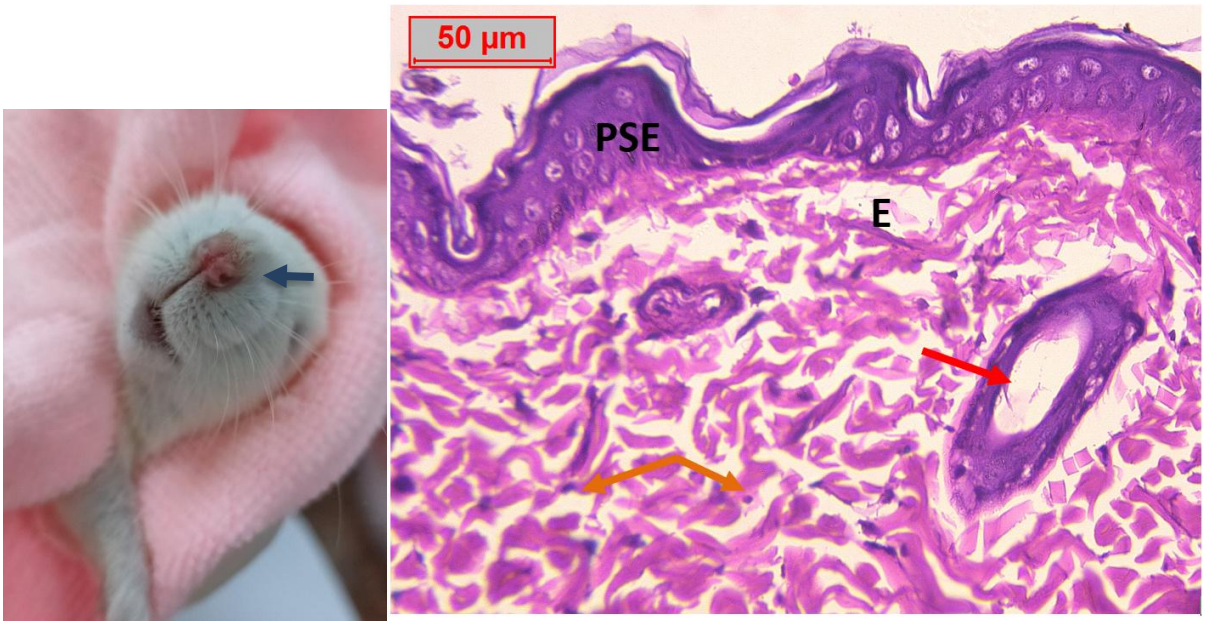


Figure 19: A photography of the nose of the **Liquorice EtOAc nano-sponge preparation group**: Blue arrow points to minimal oedema skin of the nostrils, but preserving the patency of the nasal orifice. Photomicrography of nasal tissue of the same group, shows that the nasal cavity is lined by pseudostratified epithelium (PSE) which shows normal appearance , average number of goblet cells , The lamina propria has minimal inflammatory cell infiltration (Orange arrows), with decreased edema (E) and average thickness and normal appearance of blood vessels (Red arrow). (H&E 400x)

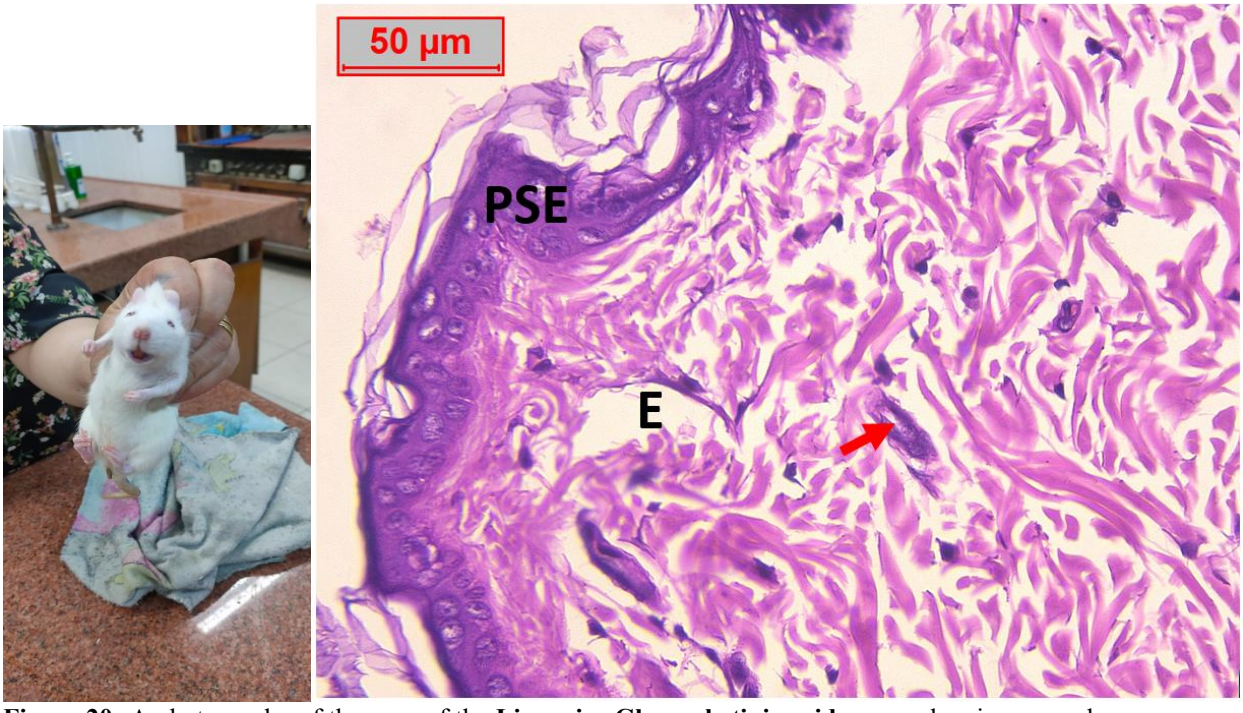


Figure 20: A photography of the nose of the **Liquorice Glycyrrhetinic acid group** showing normal appearance of nostrils. A photomicrography of nasal tissue of the same group, shows that the nasal cavity is lined by normal looking pseudostratified epithelium (PSE), average number of goblet cells , The lamina propria has no inflammatory cell infiltration, with minimal edema (E) and normal looking blood vessels (Red arrow) (H&E 400x).

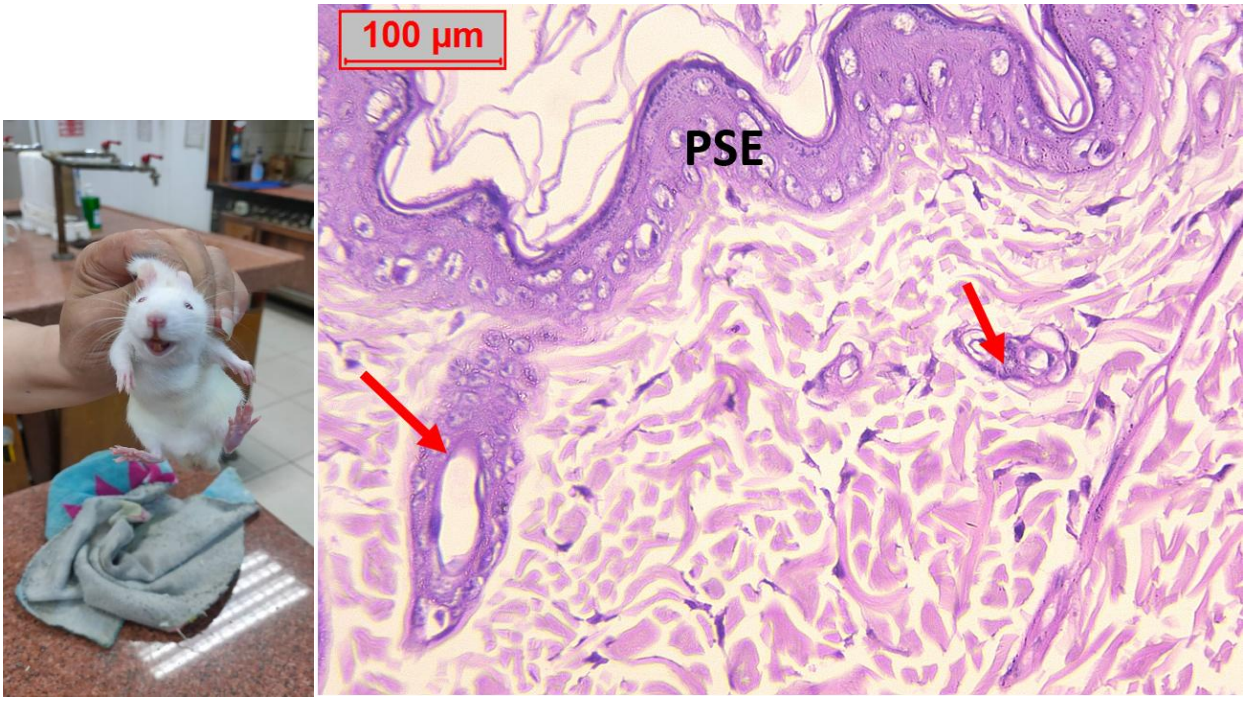


Figure 21: A photography of the nose of the **Liquorice Glycyrrhetinic acid Functionalized nano-sponge group** showing normal appearance of nostrils. A photomicrography of nasal tissue of the same group, shows that the nasal cavity is lined by normal looking pseudostratified epithelium (PSE), average number of goblet cells , The lamina propria has no inflammatory cell infiltration, nor edema and normal looking blood vessels (Red arrow). (H&E 400x)

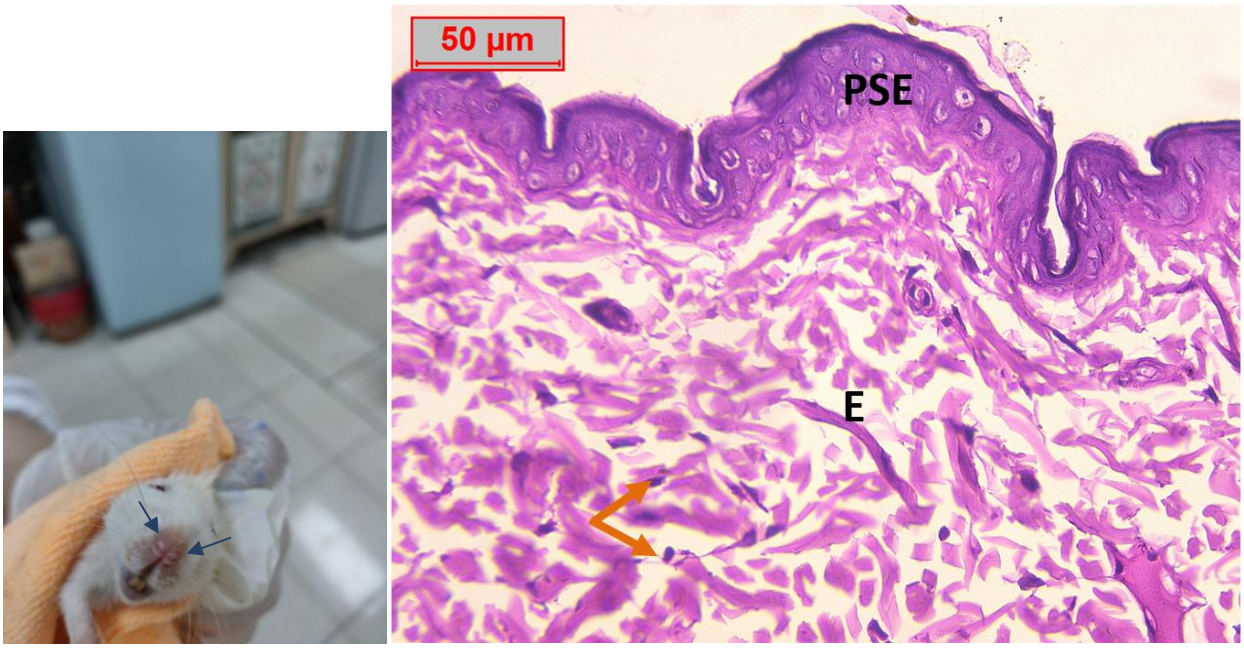


Figure 22: A photography of the nose of **Blank group**: Blue arrows point to moderate oedema of the skin of the nostrils narrowing the nasal orifices. Photomicrography of nasal tissue of the same group, shows that the nasal cavity is lined by pseudostratified epithelium (PSE) which shows normal appearance , average number of goblet cells. The lamina propria has minimal inflammatory cell infiltration (Orange arrows), with decreased oedema (E) and vascular congestion. (H&E 400x).

4. Discussions

The comprehensive metabolomic and phytochemical profiling of *Glycyrrhiza glabra* validates its longstanding ethnopharmacological reputation as a multifunctional medicinal plant with potent anti-inflammatory, antioxidant, and immunomodulatory activities. The identified metabolites including triterpene saponins, flavonoids, phenolic acids, and chalcones support the plant's traditional applications in treating respiratory, hepatic, and inflammatory disorders [57]. Moreover, sequential solvent extraction demonstrated that metabolite distribution was highly dependent on polarity. Polar fractions contained carbohydrates, tannins, and flavonoids, while non-polar fractions were enriched with sterols and triterpenes. Such chemical variability underlies the differential pharmacological effects reported for aqueous versus ethanolic extracts, which are often used for mucosal soothing and anti-inflammatory purposes in traditional medicine [58]. Glycyrrhetinic acid (GA), the principal bioactive derivative of glycyrrhizin, was efficiently isolated and structurally confirmed by NMR and LC-MSMS. These structural features align well with the literature-reported data for glycyrrhetinic acid [54], whose IUPAC name is (3β)-3-hydroxy-11-oxo-olean-12-en-30-oic acid. Accordingly, based on these observations, the identity of the compound was confidently confirmed in Figures (S1&1). LC-MSMS analysis of glycyrrhetinic acid ($C_{30}H_{46}O_4$) revealed characteristic fragmentation patterns in both positive and negative ionization modes, confirming its structural identity. In the positive mode, a prominent protonated molecular ion $[M+H]^+$ was detected at *m/z* 469.3312 (calculated *m/z* 469.3324; 2.4740 ppm error). The major fragment ion at *m/z* 425.3427 [$C_{29}H_{45}O_2$] corresponded to a neutral loss of CO2 (44 Da), indicating decarboxylation of the triterpenoid carboxyl group, which is an expected behavior for pentacyclic triterpenes. In the negative mode, a deprotonated molecular ion $[M–H]^-$ was observed at *m/z* 471.3458 (calculated *m/z* 471.3469; -2.3162 ppm), consistent with the formula $C_{30}H_{47}O_4$. The principal fragment at *m/z* 453.3368 [$C_{30}H_{45}O_3$] resulted from dehydration (−18 Da), reflecting the loss of a hydroxyl group. The obtained fragmentation profile in both modes aligns well with previously reported spectra of glycyrrhetinic acid, confirming its structural integrity and purity within the EtOAc extract. The metabolite profile obtained highlights the chemical complexity and richness of liquorice roots, characterized by the co-occurrence of flavonoid-derived metabolites and triterpene saponins. The identification of early-eluting phenolic acids agrees with previous reports describing phenolic signatures in *Glycyrrhiza* species. Fragment ions of caffeic acid, gallic acid, and tryptophan reflected classical fragmentation behavior [48]. The fragmentation of isoflavones, flavones, and chalcones between RT 7–10 min was characterized by dominant aglycone ions and neutral losses of glucose, in agreement with [53]. The fragment m/z 255 generated from iso-liquiritigenin represents a key marker for chalcone flavanone interconversion, as previously described by [50]. The presence of numerous glycosylated flavonoids between RT 15–30 min, showing sequential losses of apiose and glucose, confirms extensive glycosylation patterns in liquorice roots. The consistent appearance of the liquiritigenin aglycone (m/z 255) supports its role as a core structural unit. Diagnostic fragments of shaftoside and vicenin-2 correspond to cross-ring cleavages typical of C-glycosyl flavones [51, 52]. The detection of multiple liquorice glycoside isomers at RT 26–33 min highlights the occurrence of positional and structural isomerism, which is a well-known feature of liquorice metabolite profiles. The presence of licuroside further supports this chemical diversity. Triterpene saponins identified between RT 30-42 min represent the characteristic oleanane-type constituents of Liquorice roots. Glycyrrhizin, confidently identified by its accurate mass and diagnostic fragment at m/z 351, confirms the presence of

multiple glycosidic linkages and represents a key marker compound. The late elution of glucoliquiritin apioside suggests strong chromatographic retention due to multiple sugar substitutions and possible isomerization, consistent with previous Liquorice metabolomics studies [51]. Altogether, the co-occurrence of flavonoid glycosides and triterpenoid saponins represents the dual chemical signature of liquorice roots. The identification of multiple glycoside isomers highlights the structural complexity that may contribute to differential bioactivity (Table 3). Overall, the comprehensive annotation of 62 metabolites, supported by high mass accuracy (±3-5ppm) and diagnostic fragmentation patterns, confirms the dual chemical signature of liquorice roots, integrating flavonoid glycosides and triterpenoid saponins. This structural diversity likely underpins the broad spectrum of biological activities attributed to liquorice and provides a solid chemical basis for future bioactivity-guided and mechanistic studies (Figure 23).

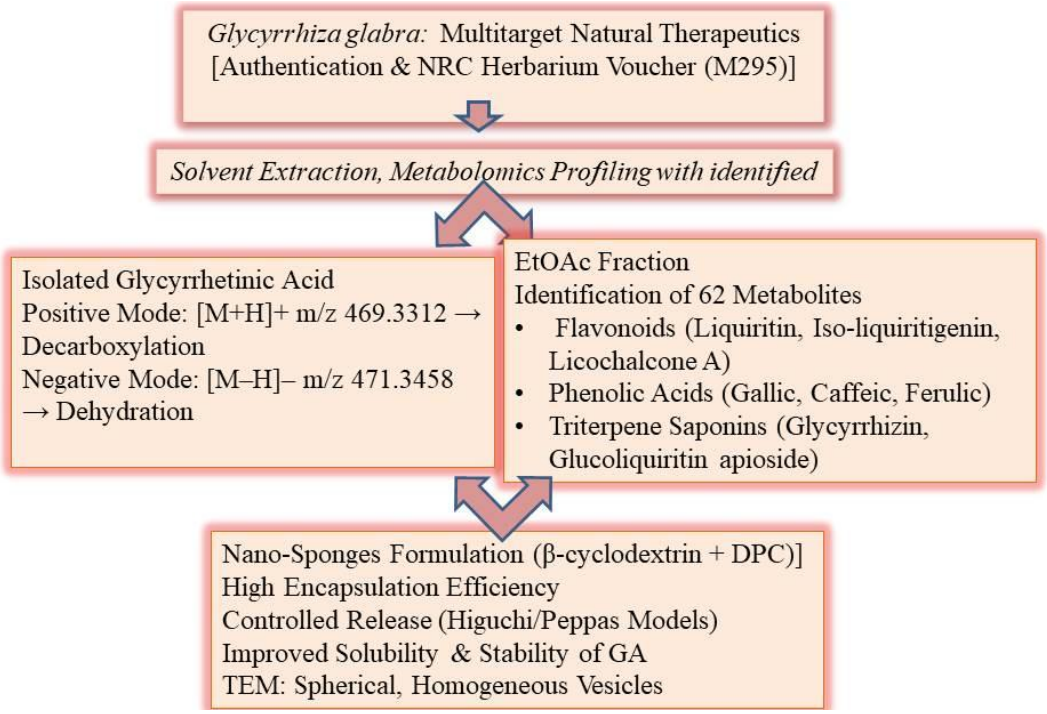


Figure 23: *Glycyrrhiza glabra* Bioactivity.

Its oleanane-type triterpenoid scaffold with hydroxyl, carbonyl, and carboxyl functionalities accounts for its broad pharmacological actions. Recent reviews highlight GA's multitarget mechanisms particularly the inhibition of 11β-hydroxysteroid dehydrogenase type 2 (11β-HSD2), suppression of NF-κB and MAPK pathways, and modulation of cytokine cascades [58]. These properties explain its cortisone-like effects without the adverse outcomes of synthetic corticosteroids. In parallel, untargeted UPLC-HRMS profiling revealed an abundance of bioactive phenolic acids (gallic, caffeic, ferulic), flavonoids (liquiritin, isoliquiritigenin, licochalcone A), and triterpenoid saponins. These secondary metabolites contribute synergistically to Liquorice's antioxidant and hepatoprotective actions by regulating redox-sensitive transcription factors such as Nrf2 and AP-1 [23]. The coexistence of glycosylated flavonoids and saponins likely enhances compound solubility, absorption, and membrane permeability, resulting in greater bioefficacy *in vivo*. This synergism between phenolic antioxidants and triterpenes represents a hallmark of *G. glabra* pharmacology. Phenolics

scavenge reactive oxygen species and modulate signaling cascades, while triterpenes act as enzyme inhibitors and membrane stabilizers, collectively mitigating oxidative and inflammatory stress. Such integrative effects justify the use of Liquorice in respiratory and dermatological formulations. Furthermore, modern delivery strategies such as β-cyclodextrin-based nanosponges address the physicochemical limitations of GA, improving solubility, stability, and sustained release. During the last decade, numerous attempts have been made to improve the preparation and application of nano-sponges. Cyclodextrin-based nano-sponges have gained the most focus and are the subject of extensive research [59]. Cyclodextrins are biodegradable, flexible chemicals utilized to improve the physico-chemical and pharmacological properties of given medicinal molecules [60]. Among the different types of natural cyclodextrins, β-cyclodextrin has the highest complexing ability and stability with crosslinking agents. Cyclodextrins also provide advantages for NSs preparation in terms of cavity size, low manufacturing costs, and increased productivity [61]. For NSs formulations, a variety of crosslinking agents have been investigated, including carbonyl diimmidazole, hexamethylenediisocynate, toluelyldianhydride, diisocynate, or carbonate and diphenyl carbonate [61]. DPC was selected as a cross-linker in our study due to its low lineal photodegradation, lack of skin irritation, and sensitization [38]. The consistently high encapsulation efficiency confirms the successful formulation of Liquorice nano-sponges. The strong crosslinking between HP-βCD and DPC likely contributed to this efficiency by facilitating greater incorporation of Liquorice within both the nano-sponges matrix and the cyclodextrin cavity [62]. The higher encapsulation efficiency observed at the 1:4 molar ratio may be attributed to optimal crosslinking that involves inclusion and external interactions simultaneously, allowing for a larger amount of extract to be encapsulated within the nano-sponges matrix and cyclodextrin cavity [38]. The observed differences in loading capacity indicate that the complexation efficiency of nano-sponges is influenced by the degree of crosslinking. At the 1:1 molar ratio, there may not be enough nanochannels available for guest complexation due to the low degree of cross-linking, which limits the encapsulation of larger quantities of Liquorice extract. The increase in vesicle size with increasing crosslinking molar ratio agrees with previous findings [63]. The low PDI values reflect uniform and narrow size distribution, indicating formulation homogeneity and stability. The highly negative zeta potential values suggest strong electrostatic repulsion between vesicles, preventing aggregation. This negative surface charge is likely attributed to free hydroxyl groups of HP-β-CD and carbonyl groups of DPC [64, 65]. TEM observations further confirmed the formation of spherical, homogeneous nano-sponges. The ultrasonic-assisted method produced vesicles with uniform size distribution, porous structure, and crystalline characteristics, consistent with previous [66]. The characteristic FT-IR bands observed for HP-βCD, DPC, and EPI-βCD are consistent with previously reported spectra [40, 67-69]. The functional groups detected in the Liquorice EtOAc extract correspond to methyl, methylene, and aromatic moieties present in sugars, proteins, amino acids, fatty acids, and phenolic compounds [69]. The shifts and broadening of characteristic FT-IR peaks in the optimized nano-sponges formulations (L3 and L4) confirm interactions between the Liquorice extract or glycyrrhetinic acid and nano-sponges components, indicating successful encapsulation [40]. The biphasic release profile observed is typical of nano-sponges systems. The initial burst release is likely due to Liquorice molecules located on the nano-sponges surface as non-inclusion complexes, either adsorbed or loosely encapsulated, while the subsequent phase represents controlled release from the nano-sponges matrix [20].The significantly higher release in alkaline medium may be attributed to enhanced solubility of Liquorice constituents, particularly flavonoids and triterpenes, under alkaline conditions

compared to acidic environments [70] The better fitting of release data to Higuchi's model indicates diffusion-controlled release behavior. According to Peppas' theory, the obtained release exponent (n) values (< 0.43) confirm that glycyrrhetinic acid release from the nano-sponges is predominantly governed by Fickian diffusion [71, 72]. Our nanosponge formulation exhibited ideal nanoscale particle size, negative zeta potential, and high entrapment efficiency, which correlate with enhanced bioavailability and reduced irritation potential. These findings align with recent formulation advances reported for phytosteroids and triterpenoid drugs designed for topical and mucosal applications [58].

In the current study, mechanical injury to the dorsal skin of rats was induced by sterilized needle tip, also nasal inflammation was induced by capsaicin [44], which led to severe inflammation manifested by redness and oedema of external tissue. [73] stated that the process of hyper-keratinization during wound healing is preceded by inflammation, which was manifested during grading the curative effect of treatment with both liquorice EtOAc preparations and both Glycyrrhrtinic acid preparations in our study.

In our study, liquorice was used topically to cure dermal and nasal lesions. It was selected on basis of previous studies, which suggested that liquorice was considered as an anti-inflammatory agent due to its ability to suppress and inhibit inflammatory pathways, as a result of its high content of bioactive anti-inflammatory compounds like glycyrrhetinic acid and glycyrrhizin preparations [74].

That's why the possible targeted immune-modulatory pathways of liquorice were studied in the present work. Its effects on ICAM-1, IL-4 and LTB-4 were studied, as these biomarkers were elevated in the untreated rats, in response to either mechanical trauma by scratching, or chemical irritation of the nose-which is part of the upper respiratory airway- by using capsiacin.

ICAM-1 which is a transmembrane glycoprotein and is a member of the immunoglobulin superfamily, is found at baseline in various cell types and is elevated in response to specific inflammatory reactions [75], was elevated in our study in the untreated rats that were exposed to injury. Also, in the study of [76], capsaicin caused expression of ICAM-1 which is an endothelial adhesion molecule that plays an important role in inflammatory reactions[76], this explains the significant elevation of ICAM-1 levels in the untreated group in the present study. Additionally, [77], reported in their study that ICAM-1 increased in rats suffering from respiratory airways inflammation, and suggested that the biomarkers of upper and lower respiratory inflammatory and allergic diseases were reduced, by treatment that decreased the level of ICAM-1 in rat sera [77]. This confirms that ICAM-1 was a target for the liquorice in the present study (Figure 23).

.

Interleukin-β4 is a type of cytokine that is produced in response to inflammation by mast cells and basophils [78]. In the current study, the level of IL-β4 was significantly elevated in the untreated groups that were subjected to induction of inflammation. On the other hand, it was reduced significantly in the treated groups with liquorice, which may point to the mode of anti-inflammatory activity of this natural product, via counteracting IL-β4 pathway. This can be explained by the hypothesis that blocking IL-β4 pathway is the target of many therapeutics, that aim to treat dermal inflammation and respiratory hypersensitivity diseases [79].

Zhang et al in their study, suggested that the anti-inflammatory activity of Glycyrrhizin which is one of the bioactive components of liquorice, is exhibited via inhibition of phospholipase A2/arachidonic acid (PLA2/ARA) pathway metabolites, including prostaglandin-

E2, thromboxane 2 and leukotriene B4 [80]. This explains the therapeutic effect of liquorice in the current study.

Collectively, these findings establish *Glycyrrhiza glabra* as a rich source of multitarget natural therapeutics. The integration of metabolomic profiling with nanosponge formulation demonstrates a modern translational approach to enhance the pharmacological potential of traditional remedies. The strong correlation between metabolite diversity, antioxidant potential, and *in vivo* anti-inflammatory effects, confirms that the pharmacological value of liquorice arises from synergistic interactions between its phyto-constituents rather than from single-molecule effects.

Conclusion

The present study highlights the potential of Liquorice extracts and glycyrrhetinic acid as promising natural anti-inflammatory agents, with local therapeutic efficacy, to avoid systemic side effects, liquorice formulations were administered topically on skin and intranasally.

They effectively exhibited anti-inflammatory effects, while avoiding exposure to undesired corticosteroid-related complications. These findings support the employment of glycyrrhetinic acid-based formulations, as safe and efficient alternatives for managing inflammation and related disorders.

Footnotes

1.The current study was done as a complementary study to the former study, that had been published in the "Inflammopharmacology" journal under title: "A pharmaco-metabolomics study of Glycyrrhiza glabra, Boswellia sarca, and Acacia nilotica in acute allergic dermatitis".

2.The current study is done as a part of the project entitled "Pharmacological investigation and Metabolomics study of promising anti-inflammatory herbal oils loaded in a polymeric nano-composite drug delivery system targeting Dermatitis and Upper Respiratory Allergy in rats", under registration number 12060132.

3.Glycyrrhiza glabra was selected to study the effect of its ethyl acetate extracts and nanosponge loaded ethyl acetate extracts as well as Glycyrrhetinic acid (GA) and its functionalized nanosponge formulation on corporal dermal and nasal inflammation.

4.The reason for selection of Glycyrrhiza glabra in the current study- rather than the other studied natural products in the previous study-was that it exhibited promising therapeutic anti-inflammatory activity with neglectable side effects, besides being locally available with affordable cost in the local market as well as its good taste, which makes it more acceptable for consumption by the local population enhancing its compliance for future introduction in clinical trials and accreditation as a therapeutic multipurpose anti-inflammatory supplement.

5.The nanosponge delivery system facilitated the absorption of EtOAc and GA and exhibited promising effect.

Declarations

Ethics approval: This study adhered to contemporary ethical standards, addressing issues such as plagiarism, misconduct, data fabrication, falsification, duplicate publication, and redundancy. All animal experiments complied with the *National Guide for the Care and Use of Laboratory Animals*, NIH publication 86-23 (revised 1985), and the guidelines of the Academy of Sciences. Approval was obtained from the Institutional Animal Ethical Committee (IAEC) in accordance

with National Regulations of Animal Welfare. The Research Centre Ethics Committee approval number (16/138) provided clearance for the study.

A Funding Declaration: Funding of the experimental work was obtained from the "In house project unit of National Research Centre, Dokki, Egypt", for the project entitled "Pharmacological investigation and Metabolomics study of promising anti-inflammatory herbal oils loaded in a polymeric nano-composite drug delivery system targeting Dermatitis and Upper Respiratory Allergy in rats", under registration number 12060132.

Open access funding was provided by the Science, Technology & Innovation Funding Authority (STDF) in co-operation with the Egyptian Knowledge Bank (EKB).

Consent to participate: Not applicable as the study doesn't involve human individuals. It was done only on animals.

Consent for Publication: All authors of the current work, agree to have this article published in your journal

Availability of Data and Materials: All data generated or analyzed during this study are included in this published article (and its supplementary information files). Additional datasets are available from the corresponding author upon reasonable request.

Conflict of interest: The authors declare that they have no conflict of interest.

Author Contributions Statement

MAM is the co-principal investigator of the project, she contributed to conceptualization, plant selection, extraction, and metabolomics analysis, and was responsible for methodology, investigation, data curation, as well as drafting, reviewing, and editing the manuscript. ***ABD*** contributed to conceptualization, methodology, investigation, formal analysis, data curation, and writing (original draft, review, and editing). ***NNY*** was responsible for histopathological methodology, formal analysis, and writing. ***AFH*** and ***SAG*** contributed to biochemical methodology and formal analysis. ***SAT*** contributed to conceptualization, methodology, investigation, and data curation. ***BMMI*** is the principal investigator of the project, she contributed to conceptualization, methodology, investigation, data curation, and drafting, reviewing, and editing of the in vivo pharmacological study. All authors wrote the paper draft, while ***MAM*** corrected the final form of the draft. ***MAM*** and ***BMMI*** supervised the experimentations. All experiments were performed by all authors. All data were generated in-house, and no paper mill was used. All authors agree to be accountable for all aspects of the work, ensuring integrity and accuracy.

Acknowledgements: The authors thank the National Research Centre (NRC) for providing the necessary facilities and technical support for this work. We gratefully acknowledge Prof. Dr. Hab. Piotr Kachlicki, Institute of Plant Genetics, Polish Academy of Sciences (PAS), Poznań, for his support with UPLC/HRMS analysis.

References

1. Kim, S.-W., et al., *Glycyrrhizic acid affords robust neuroprotection in the postischemic brain via anti-inflammatory effect by inhibiting HMGB1 phosphorylation and secretion.* Neurobiology of disease, 2012. **46**(1): p. 147-156.
2. Dhingra, D. and A. Sharma, *Antidepressant-like activity of Glycyrrhiza glabra L. in mouse models of immobility tests.* Progress in Neuro-Psychopharmacology and Biological Psychiatry, 2006. **30**(3): p. 449-454.
3. Laconi, S., M.A. Madeddu, and R. Pompei, *Autophagy activation and antiviral activity by a licorice triterpene.* Phytotherapy Research, 2014. **28**(12): p. 1890-1892.
4. Montoro, P., et al., *Metabolic profiling of roots of liquorice (Glycyrrhiza glabra) from different geographical areas by ESI/MS/MS and determination of major metabolites by LC-ESI/MS and LC-ESI/MS/MS.* Journal of pharmaceutical and biomedical analysis, 2011. **54**(3): p. 535-544.
5. Huo, M., et al., *Kansui-liquorice enhances the "water-expelling" effect of Gansui Banxia decoction in rats with malignant ascites by targeting the NPs/NPRs/cGMP/PKGII pathway and T cell immunity.* Frontiers in Pharmacology, 2025. **16**: p. 1557717.
6. Dang, L., et al., *Licorice: comprehensive review of its chemical composition, pharmacodynamics, and medicinal value.* Acupuncture and Herbal Medicine, 2024. **4**(1): p. 136-150.
7. Nascimento, M.H.M.d. and D.R. de Araújo, *Exploring the pharmacological potential of glycyrrhizic acid: From therapeutic applications to trends in nanomedicine.* Future Pharmacology, 2022. **2**(1): p. 1-15.
8. Monder, C. and P.C. White, *11β-Hydroxysteroid dehydrogenase.* Vitamins & Hormones, 1993. **47**: p. 187-271.
9. Hall, L. and R. Hart, *Role of corticosteroids in skin physiology and therapeutic potential of an 11β-HSD1 inhibitor: A review.* International Journal of Dermatology, 2024. **63**(4): p. 443-454.
10. Stewart, P., et al., *Mineralocorticoid activity of liquorice: 11-beta-hydroxysteroid dehydrogenase deficiency comes of age.* The Lancet, 1987. **330**(8563): p. 821-824.
11. Conn, J.W., D.R. Rovner, and E.L. Cohen, *Licorice-induced pseudoaldosteronism: hypertension, hypokalemia, aldosteronopenia, and suppressed plasma renin activity.* Jama, 1968. **205**(7): p. 492-496.
12. Mali, A., R. Bathe, and M. Patil, *An updated review on transdermal drug delivery systems.* International Journal of Advances in Scientific Research, 2015. **1**: p. 244.
13. Soares, P., et al., *Design and engineering of magneto-responsive devices for cancer theranostics: Nano to macro perspective.* Progress in Materials Science, 2021. **116**: p. 100742.
14. Rossi, S., et al., *Characterization of chitosan hydrochloride–mucin interaction by means of viscosimetric and turbidimetric measurements.* European Journal of Pharmaceutical Sciences, 2000. **10**(4): p. 251-257.
15. Munin, A. and F. Edwards-Lévy, *Encapsulation of natural polyphenolic compounds; a review.* Pharmaceutics, 2011. **3**(4): p. 793-829.
16. Wadhwa, G., et al., *Essential oil–cyclodextrin complexes: an updated review.* Journal of Inclusion Phenomena and Macrocyclic Chemistry, 2017. **89**(1): p. 39-58.
17. Szejtli, J., *Past, Present, and Future of Cyclodextrin Research.* Pure and Applied Chemistry - PURE APPL CHEM, 2004. **76**: p. 1825-1845.
18. Swaminathan, S., et al., *Structural evidence of differential forms of nanosponges of beta-cyclodextrin and its effect on solubilization of a model drug.* Journal of Inclusion Phenomena and Macrocyclic Chemistry, 2013. **76**(1): p. 201-211.
19. Patel, E. and R. Oswal, *Nanosponge and micro sponges: a novel drug delivery system.* Int J Res Pharm Chem, 2012. **2**(2): p. 237-244.
20. Swaminathan, S., et al., *Cyclodextrin-based nanosponges encapsulating camptothecin: physicochemical characterization, stability and cytotoxicity.* European Journal of Pharmaceutics and Biopharmaceutics, 2010. **74**(2): p. 193-201.
21. Ibrahim, B., et al., *Phytochemical and pharmacological studies on newly-suggested herbal formulations for potential protection against inflammatory conditions.* Int. J. Pharmacogn. Phytochem. Res, 2016. **8**: p. 2044-2055.
22. Taleb, S.A., et al., *Development and in vitro/in vivo evaluation of a nanosponge formulation loaded with Boswellia carterii oil extracts for the enhanced anti-inflammatory activity for the management of respiratory allergies.* Journal of Pharmaceutical Investigation, 2024. **54**(5): p. 643-665.
23. Mahrous, R.S., R.S. Ibrahim, and H. Fathy, *Unveiling Liquorice: A sweet journey through history, phytochemistry, and exceptional pharmacological activities.* Journal of Advanced Pharmaceutical Sciences, 2025: p. 28-58.

24. Ibrahim, B.M., et al., *A pharmaco-metabolomics study of Glycyrrhiza glabra, Boswellia sarca, and Acacia nilotica in acute allergic dermatitis.* Inflammopharmacology, 2025: p. 1-22.
25. Guenther, E., *The essential oils. Vol. 5.* The essential oils. Vol. 5., 1952.
26. Lewis, D. and D. Smith, *SUGAR ALCOHOLS (POLYOLS) IN FUNGI AND GREEN PLANTS: II. METHODS OF DETECTION AND QUANTITATIVE ESTIMATION IN PLANT EXTRACTS.* New Phytologist, 1967. **66**(2): p. 185-204.
27. Shellard, E.J., *Practical plant chemistry for pharmacy students*. 1957: Pitman Medical.
28. Harborne, J., *Phytochemicals methods.* London: Hapman and Hall Ltd, 1973: p. 49-188.
29. Shinoda, J., *Color reactions of flavone and flavonol derivatives and the like.* J Pharm Soc Jpn, 1928. **48**: p. 214-220.
30. HANSON, J., *THE DI-AND SESTERTERPENES PART 1: THE DITERPENES.* Chemistry of Terpenes and Terpenoids, 1972: p. 155.
31. Piasecka, A., et al., *Combined mass spectrometric and chromatographic methods for in-depth analysis of phenolic secondary metabolites in barley leaves.* Journal of Mass Spectrometry, 2015. **50**(3): p. 513-532.
32. Mohammed, M.A., et al., *Comprehensive Metabolomic, Lipidomic and Pathological Profiles of Baobab (Adansonia digitata) Fruit pulp Extracts in Diabetic Rats.* Journal of Pharmaceutical and Biomedical Analysis, 2021: p. 114139.
33. Tsugawa, H., et al., *MS-DIAL 4: accelerating lipidomics using an MS/MS, CCS, and retention time atlas.* bioRxiv, 2020.
34. Ammar, N.M., et al., *Metabolomic profiling to reveal the therapeutic potency of Posidonia oceanica nanoparticles in diabetic rats.* RSC Advances, 2021. **11**(14): p. 8398-8410.
35. Trotta, F., et al., *Ultrasound-assisted synthesis of cyclodextrin-based nanosponges*. 2008, Google Patents.
36. Abou Taleb, S., et al., *Investigation of a new horizon antifungal activity with enhancing the antimicrobial efficacy of ciprofloxacin and its binary mixture via their encapsulation in nanoassemblies: in vitro and in vivo evaluation.* Drug Dev Res, 2019.
37. Asfaram, A., M. Ghaedi, and K. Dashtian, *Ultrasound assisted combined molecularly imprinted polymer for selective extraction of nicotinamide in human urine and milk samples: Spectrophotometric determination and optimization study.* Ultrasonics Sonochemistry, 2017. **34**: p. 640-650.
38. Kumar, S., et al., *Encapsulation of Babchi Oil in Cyclodextrin-Based Nanosponges: Physicochemical Characterization, Photodegradation, and In Vitro Cytotoxicity Studies.* Pharmaceutics, 2018. **10**: p. 169.
39. Abou Taleb, S., et al., *Quercitrin loaded cyclodextrin based nanosponge as a promising approach for management of lung cancer and COVID-19.* J Drug Deliv Sci Technol, 2022. **77**: p. 103921.
40. Taleb, S.A., et al., *Development and in vitro/in vivo evaluation of a nanosponge formulation loaded with Boswellia carterii oil extracts for the enhanced anti-inflammatory activity for the management of respiratory allergies.* Journal of Pharmaceutical Investigation, 2024. **54**(5): p. 643-665.
41. Shimada, K., et al., *Antioxidative properties of xanthan on the autoxidation of soybean oil in cyclodextrin emulsion.* Journal of agricultural and food chemistry, 1992. **40**(6): p. 945-948.
42. Dinkova-Kostova, A., et al., *Phenolic Michael reaction acceptors: combined direct and indirect antioxidant defenses against electrophiles and oxidants.* Medicinal Chemistry, 2007. **3**(3): p. 261-268.
43. Chemicals, D., *OECD Guideline for testing of chemicals.* The Organisation for Economic Co-operation and Development: Paris, France, 2005: p. 1-13.
44. Kalogjera, L., et al., *Dose-dependent protective effect of BPC 157 on capsaicin-induced rhinitis in rats.* European Archives of Oto-Rhino-Laryngology, 1997. **254**(Suppl 1): p. S9-S11.
45. Sorg, D.A. and B. Buckner, *A simple method of obtaining venous blood from small laboratory animals.* Proceedings of the Society for Experimental Biology and Medicine, 1964. **115**(4): p. 1131-1132.
46. Drury, R. and E. Wallington, *Carleton's histological technique 5th ed.* New York: Churchill Livingstone, 1980: p. 270.
47. Mohammeda, M.A., et al., *IN VITRO SCREENING OF ANNONA CHERIMOLA LEAVES AND BARK FOR THEIR ANTIOXIDANT ACTIVITY AND IN VIVO ASSESSMENT AS PROTECTIVE AGENTS AGAINST GASTRIC ULCER IN RATS.*
48. Hamad, G., et al., *Chemical composition, antioxidant, antimicrobial and anticancer activities of licorice (Glycyrrhiza glabra L.) root and its application in functional yoghurt.* J. Food Nutr. Res, 2020. **8**(12): p. 707-715.
49. Khalaf, I., et al., *HPLC-MS study of phytoestrogens from Glycyrrhiza glabra.* Farmacia, 2010. **58**(1): p. 89-94.

50. Xie, J., et al., *Identification and simultaneous determination of glycyrrhizin, formononetin, glycyrrhetinic acid, liquiritin, isoliquiritigenin, and licochalcone A in licorice by LC-MS/MS.* Acta Chromatographica, 2014. **26**(3): p. 507-516.
51. Wang, Y., et al., *UPLC–Q-TOF-MS/MS fingerprinting of traditional chinese formula SiJunZiTang.* Journal of Pharmaceutical and Biomedical Analysis, 2013. **80**: p. 24-33.
52. Montero, L., et al., *Metabolite profiling of licorice (Glycyrrhiza glabra) from different locations using comprehensive two-dimensional liquid chromatography coupled to diode array and tandem mass spectrometry detection.* Analytica Chimica Acta, 2016. **913**: p. 145-159.
53. Wang, S., et al., *Fragment ion diagnostic strategies for the comprehensive identification of chemical profile of Gui-Zhi-Tang by integrating high-resolution MS, multiple-stage MS and UV information.* Journal of pharmaceutical and biomedical analysis, 2014. **98**: p. 22-35.
54. Chaturvedula, V.S.P., O. Yu, and G. Mao, *Isolation and NMR spectral assignments of 18-glycyrrhetinic acid-3-Od-glucuronide and 18-glycyrrhetinic acid.* IOSR J Pharm, 2014. **4**(5).
55. Koga, K., et al., *Determination of 18α-glycyrrhizin and 18β-glycyrrhizin in dog plasma by high-performance liquid chromatography.* Journal of Chromatography B: Biomedical Sciences and Applications, 2000. **738**(1): p. 165-168.
56. Kitagawa, I., et al., *Saponin and sapogenol. XLVIII. On the constituents of the roots of Glycyrrhiza uralensis Fischer from northeastern China.(2). Licorice-saponins D3, E2, F3, G2, H2, J2, and K2.* Chemical and pharmaceutical bulletin, 1993. **41**(8): p. 1337-1345.
57. Chen, L., et al., *A review of typical biological activities of glycyrrhetinic acid and its derivatives.* RSC advances, 2024. **14**(10): p. 6557-6597.
58. Shao, L., et al., *New insights of licorice (Glycyrrhiza genus) as a functional food.* Food Chemistry, 2025: p. 145332.
59. Tejashri, G., B. Amrita, and J. Darshana, *Cyclodextrin based nanosponges for pharmaceutical use: a review.* Acta Pharm, 2013. **63**(3): p. 335-58.
60. Loftsson, T. and M.E. Brewster, *Pharmaceutical applications of cyclodextrins. 1. Drug solubilization and stabilization.* J Pharm Sci, 1996. **85**(10): p. 1017-25.
61. Ibrahim, B.M.M., et al., *Appraisal terpenoids rich Boswellia carterri ethyl acetate extract in binary cyclodextrin oligomer nano complex for improving respiratory distress.* Sci Rep, 2024. **14**(1): p. 16779.
62. Olteanu, A.A., et al., *Effect of β-cyclodextrins based nanosponges on the solubility of lipophilic pharmacological active substances (repaglinide).* Journal of Inclusion Phenomena and Macrocyclic Chemistry, 2014. **80**(1): p. 17-24.
63. Yaşayan, G., et al., *Fabrication and characterisation studies of cyclodextrin-based nanosponges for sulfamethoxazole delivery.* Journal of Inclusion Phenomena and Macrocyclic Chemistry, 2020. **97**(3): p. 175-186.
64. Omar, S.M., F. Ibrahim, and A. Ismail, *Formulation and evaluation of cyclodextrin-based nanosponges of griseofulvin as pediatric oral liquid dosage form for enhancing bioavailability and masking bitter taste.* Saudi Pharmaceutical Journal, 2020. **28**(3): p. 349-361.
65. Zidan, M.F., et al., *In vitro and in vivo evaluation of cyclodextrin-based nanosponges for enhancing oral bioavailability of atorvastatin calcium.* Drug Development and Industrial Pharmacy, 2018. **44**(8): p. 1243-1253.
66. Mahalingam, S., et al., *Synthesis and Characterization of Chrysin-Loaded β -Cyclodextrin-Based Nanosponges to Enhance In-Vitro Solubility, Photostability, Drug Release, Antioxidant Effects and Antitumorous Efficacy.* Journal of Nanoscience and Nanotechnology, 2017. **17**: p. 8742-8751.
67. Dubey, P., et al., *Formulations and evaluation of Cyclodextrin complexed Ceadroxil loaded nanosponges.* International Journal of Drug Delivery, 2017. **9**: p. 84.
68. Raja, D., et al., *Development of a novel water-soluble β-cyclodextrin epichlorohydrin polymer complex to improve aqueous solubility.* J. Chem. Biol. Phys. Sci., 2012. **2**: p. 325-330.
69. Al Shaheen, M., *Synthesis and characterization of zinc nanoparticles by natural organic compounds extracted from Licorice root and their influence on germination of Sorghum bicolor seeds.* Jordan Journal of Biological Sciences, 2020. **13**.
70. Ohno, H., et al., *Efficient utilization of licorice root by alkaline extraction.* In Vivo, 2014. **28**(5): p. 785-94.
71. Peppas, N.A. and J.J. Sahlin, *A simple equation for the description of solute release. III. Coupling of diffusion and relaxation.* Int J Pharm, 1989. **57**(2): p. 169-172.
72. Lokhande, A.B., et al., *Preparation and characterization of repaglinide loaded ethylcellulose nanoparticles by solvent diffusion technique using high pressure homogenizer.* J Pharm Res, 2013. **7**(5): p. 421-426.

73. Jeremy, A.H., et al., *Inflammatory events are involved in acne lesion initiation.* Journal of Investigative Dermatology, 2003. **121**(1): p. 20-27.
74. Fatima, I., et al., *Exploring the Role of Licorice and Its Derivatives in Cell Signaling Pathway NF-κB and MAPK.* Journal of Nutrition and Metabolism, 2024. **2024**(1): p. 9988167.
75. F Abdou, A., et al., *Serum Intercellular Adhesion Molecule-1 in Patients with Acne Vulgaris.* Benha Journal of Applied Sciences, 2022. **7**(6): p. 41-45.
76. Járomi, P., et al., *Capsaicin-induced rapid neutrophil leukocyte activation in the rat urinary bladder microcirculatory bed.* Neurourology and Urodynamics, 2018. **37**(2): p. 690-698.
77. Ibrahim, B.M., et al., *Appraisal terpenoids rich Boswellia carterri ethyl acetate extract in binary cyclodextrin oligomer nano complex for improving respiratory distress.* Scientific Reports, 2024. **14**(1): p. 16779.
78. Hall, W.A., *Immunotoxin treatment of brain tumors.* Immunotoxin Methods and Protocols, 2001: p. 139-154.
79. Gärtner, Y., et al., *Interleukin-4 as a therapeutic target.* Pharmacology & therapeutics, 2023. **242**: p. 108348.
80. Zhang, R., et al., *Network pharmacology and in vitro experimental verification unveil glycyrrhizin from glycyrrhiza glabra alleviates acute pancreatitis via modulation of MAPK and STAT3 signaling pathways.* BMC Complementary Medicine and Therapies, 2024. **24**(1): p. 58.

Supplementary Files

This is a list of supplementary files associated with this preprint. Click to download.

- 2.Supl..docx
- floatimage1.jpeg